Reservoir-Engineered Entanglement in Multimode Optomechanics

Author:
Hasan, Monirul

Publication Date:
2016

DOI:
https://doi.org/10.26190/unsworks/19264

License:
https://creativecommons.org/licenses/by-nc-nd/3.0/au/
Link to license to see what you are allowed to do with this resource.

Downloaded from http://hdl.handle.net/1959.4/56998 in https://unsworks.unsw.edu.au on 2024-04-30

Reservoir-Engineered Entanglement in Multimode Optomechanics

Monirul Hasan

A thesis submitted in fulfilment

of the requirements of the degree of

Master by Research

School of Engineering and Information Technology

The University of New South Wales

Canberra, Australia

March 31, 2016

THE UNIVERSITY OF NEW SOUTH WALES
Thesis/Dissertation Sheet

Surname or Family name: **Hasan**
First name: **Monirul** Other name/s:
Abbreviation for degree as given in the University calendar: **Master by Research**
School: **School of Engineering and Information Technology** Faculty: **UNSW@ADFA**
Title: **Reservoir-Engineered Entanglement in Multimode Optomechanics**

Abstract 350 words maximum:

There has recently been considerable interest in the study of mechanical oscillators in the quantum regime. Coupled electromagnetic cavities have proven useful for the measurement and control of these mechanical modes. Recent experiments have demonstrated the cooling of a macroscopic mechanical oscillator to its quantum ground state via the back-action of a coupled electromagnetic cavity mode. Such experiments are motivated by the possibility of fundamental tests of the limits of quantum mechanics, for coherent interfaces for quantum information processing, and for enhanced sensing.

In this thesis we study the preparation and detection of multimode entangled states of mechanical oscillators using coupled electromagnetic cavity modes as a resource for control. It is shown that the entangled steady-states persist with experimentally accessible parameters, and they may be detected by monitoring the cavity output spectrum.

In particular, the research presented here describes a system composed of three mechanical oscillators coupled to three electromagnetic cavity modes. The electromagnetic cavity modes may take the form of optical cavities or microwave circuits. Via appropriate driving of the coupled cavity modes, we show how highly-entangled states of three mechanical oscillators can be prepared. In an adiabatic limit in which the electromagnetic cavity modes are damped rapidly compared with other system parameters, the operators describing the dissipation of the three mechanical oscillators can take the form of the *nullifiers* that define a continuous-variable *cluster state* in quantum information processing. Using this so-called reservoir engineering scheme, we describe how the mechanical oscillators can be prepared in a highly-entangled steady-state.

The effect of uncontrollable dissipation of the mechanical modes into local thermal environments has also been accounted for. The entanglement properties of the steady-state are evaluated, and the impact of the mechanical motion on the spectrum of fluctuations of the coupled electromagnetic cavity modes is determined. The bipartite entanglement between mechanical oscillators is quantified using the logarithmic negativity and the genuine tripartite mechanical entanglement is quantified using the Gaussian Rényi-2 entanglement entropy.

Declaration relating to disposition of project thesis/dissertation

I hereby grant to the University of New South Wales or its agents the right to archive and to make available my thesis or dissertation in whole or in part in the University libraries in all forms of media, now or here after known, subject to the provisions of the Copyright Act 1968. I retain all property rights, such as patent rights. I also retain the right to use in future works (such as articles or books) all or part of this thesis or dissertation.

....

Signature Witness Date

The University recognises that there may be exceptional circumstances requiring restrictions on copying or conditions on use. Requests for restriction for a period of up to 2 years must be made in writing. Requests for a longer period of restriction may be considered in exceptional circumstances and require the approval of the Dean of Graduate Research.

FOR OFFICE USE ONLY Date of completion of requirements for Award:

Originality Statement

I hereby declare that this submission is my own work and to the best of my knowledge and belief, it contains no material previously published or written by another person, nor material which to a substantial extent has been accepted for the award of any other degree or diploma at UNSW or any other educational institution, except where due acknowledgement is made in this thesis. Any contribution made to the research by colleagues, with whom I have worked at UNSW or elsewhere, during my candidature, is fully acknowledged. I also declare that the intellectual content of this thesis is the product of my own work, except to the extent that assistance from others in the project's design and conception or in style, presentation and linguistic expression is acknowledge.

Monirul Hasan

UNSW, Australia

March 31, 2016.

Authenticity Statement

I certify that the Library deposit digital copy is a direct equivalent of the final officially approved version of my thesis. No emendation of content has occurred and if there are any minor variations in formatting, they are the result of the conversion to digital format.

Monirul Hasan
UNSW, Australia
March 31, 2016.

Dedication

To my beloved mother...

Acknowledgements

Doing a Masters by Research is almost not possible without the support of numerous people around. Therefore here is the right place to award them with my appreciation.

First and foremost, I would like to express my sincere gratitude to my supervisor Dr. Matthew James Woolley, who offered me the opportunity to get involved in this very interesting research area. I like to remember all the fruitful discussions we had together. Matt was not only academic supervisor but also a mentor to me. Especially, I would like to thank him for his kind consideration and precious time on proofreading, and constructive feedbacks during my thesis writing.

I cannot wait to owe a huge thanks to my housemates Kalyan Da, Forhad Bhai, Shibli, Rashed Bhai, and Monju for their immense caring and support in all ups and downs of my life in Australia.

I would like to show my gratitude to my few phenomenally big-hearted colleagues and friends, Sajal, Humayon, Nargis Apu, Smita Apu, Mehedi Bhai, Mohammad Fuad Ezmir, Sohel Bhai, Shain Bhai, Rashed, Rossi Apu, Khaleque Bhai, Imran, Polash, Fahad, Mahi, Adnan Bhai, Shamim Bhai, Nancy, Habibullah, Bashir Bhai, Mehdi Bhai, Mehran, Ripon Da, Sumon, Barik Bhai, and a lot to mention, who have made my time at UNSW, Canberra worthwhile. I thank you all for all the great times we spent together and for all the sweet memories.

I would also like to thank Craig I. Edwards and Elvira Berra for their continuous support and guidance throughout the candidature. I am thankful to the entire UNSW school staff for arranging all necessary facilities during my presence at school.

Finally no words are adequate to thank my family for their continuous support and inspiration throughout the journey.

Abstract

There has recently been considerable interest in the study of mechanical oscillators in the quantum regime. Coupled electromagnetic cavities have proven useful for the measurement and control of these mechanical modes. Recent experiments have demonstrated the cooling of a macroscopic mechanical oscillator to its quantum ground state via the back-action of a coupled electromagnetic cavity mode. Such experiments are motivated by the possibility of fundamental tests of the limits of quantum mechanics, for coherent interfaces for quantum information processing, and for enhanced sensing.

In this thesis we study the preparation and detection of multimode entangled states of mechanical oscillators using coupled electromagnetic cavity modes as a resource for control. It is shown that the entangled steady-states persist with experimentally accessible parameters, and they may be detected by monitoring the cavity output spectrum.

In particular, the research presented here describes a system composed of three mechanical oscillators coupled to three electromagnetic cavity modes. The electromagnetic cavity modes may take the form of optical cavities or microwave circuits. Via appropriate driving of the coupled cavity modes, we show how highly-entangled states of three mechanical oscillators can be prepared. In an adiabatic limit in which the electromagnetic cavity modes are damped rapidly compared with other system parameters, the operators describing the dissipation of the three mechanical oscillators can take the form of the *nullifiers* that define a continuous-variable *cluster state* in quantum information processing. Using this so-called reservoir engineering scheme, we describe how the mechanical oscillators can be prepared in a highly-entangled steady-state.

The effect of uncontrollable dissipation of the mechanical modes into local thermal environments has also been accounted for. The entanglement properties of the steady-state are evaluated, and the impact of the mechanical motion on the spectrum of fluctuations of the coupled electromagnetic cavity modes is determined. The bipartite entanglement between mechanical oscillators is quantified using the logarithmic negativity and the genuine tripartite mechanical entanglement is quantified using the Gaussian Rényi-2 entanglement entropy.

List of Publications

Conference Papers

1. M. Hasan and M. J. Woolley, "Tripartite mechanical entanglement in quantum optomechanical systems," *Frontiers in Optics and Laser Science*, San Jose, JW2A.57 (2015).

Conference Poster

1. M. Hasan and M. J. Woolley, "Reservoir-engineered entanglement in multimode optomechanics," *EQUS Optomechanics Incubator*, Sydney, Australia (2014).

Contents

List of Figures

Chapter 1

Quantum Optomechanics

There has been a lot of recent interest in the study of macroscopic mechanical oscillators in the quantum regime, with anticipated applications in sensing, information processing and tests of fundamental physics. In particular, microwave and optical fields have been used for the measurement and control of these oscillators, creating the field of quantum optomechanics. Before considering the quantum mechanics of these systems, however, we consider the classical dynamics of a macroscopic mechanical oscillator.

1.1 Continuum Mechanics

In this section we will review the dynamics of a classical mechanical resonator. We will focus on the vibrations of a rigid body, rather than on its translation or rotation in space. The continuum mechanics of a mechanical resonator's dynamics can be classically described by a space- and time-dependent displacement field. Focusing on the lowest-lying (fundamental) mode of the resonator, for small excitation amplitudes the vibration may be considered as a linear (harmonic) oscillator, and the motional state may then be represented by a single representative position coordinate and a single representative momentum coordinate.

The description of long-wavelength vibrations, and the determination of the fundamental spatial modes of a mechanical system can be obtained through continuum mechanics. The description is valid because the wavelengths under consideration are large compared with the interatomic spacing of the underlying crystal lattice. The assumption of a linear relationship between the stress and strain fields can be considered in this approach. We shall focus on translational waves (rotationally-propagating waves have much higher frequencies, and are difficult to detect and actuate). These may be classified as: longitudinal (propagation and displacement in the same direction), transverse (displacements orthogonal to the propagation direction), or torsional (rotational displacements with translational propagation). In three-dimensional structures we are usually interested in longitudinal waves (breathing modes), while in two dimensions and in one dimension we usually focus on transverse waves of low frequency, as these are relatively easy to actuate and detect.

A displacement field $\mathbf{u}(\mathbf{r}, t)$ leads to the strain tensor [1],

$$S_{\alpha\mu}(\mathbf{r}) = \frac{1}{2}\left(\frac{\partial u_\alpha}{\partial x_\mu} + \frac{\partial u_\mu}{\partial x_\alpha}\right), \tag{1.1}$$

where u_α is the displacement along the axis $\alpha = \{1, 2, 3\}$ at the coordinate x_μ with $\mu = \{1, 2, 3\}$. The material may be described by an elastic tensor $E_{\mu\alpha\beta\nu}$, having 36 independent parameters for an assumed linear response. The stress tensor, in terms of the symmetrized elastic tensor $c_{\mu\alpha\beta\nu}$, is then

$$T_{\mu\nu} = \sum_{\alpha,\beta=1}^{3} c_{\mu\alpha\beta\nu} S_{\alpha\beta}. \tag{1.2}$$

The dynamics can be written as,

$$\rho \frac{\partial^2 \mathbf{u}(\mathbf{r}, t)}{\partial t^2} = \underline{\nabla} T + \mathbf{f}(\mathbf{r}, t), \tag{1.3}$$

where $\mathbf{f}$ is the externally applied force distribution, ρ is the density and $\underline{\nabla}$ is the

gradient of the stress field T.

In an isotropic solid, one may derive three types of wave equations, corresponding to longitudinal, transverse and torsional waves. The equation of wave propagation for linear one dimensional structure are shown in Table 1.1. For the transverse

Oscillation	Equation	Ansatz	Dispersion
Longitudinal	$\rho\frac{\partial^2 u}{\partial t^2} = E\frac{\partial^2 u}{\partial z^2}$	$u(z,t) = u_0 e^{i(qz\pm\omega t+\phi)}$	$\omega = \sqrt{\frac{E}{\rho}}\ q$
Transverse	$\rho\frac{\partial^2 u}{\partial t^2} = T\frac{\partial^2 u}{\partial z^2} - EI\frac{\partial^4 u}{\partial z^4}$	$u(z,t) = u(z)e^{-i\omega t}$; $u(z) = e^{\pm qz}, e^{\pm iqz}$	$\omega^2 = \frac{T}{\rho A}q^2 + \frac{EI}{\rho A}q^4$

Table 1.1: Wave equations for linear elastic one-dimensional structures. Note that u is the translational displacement of the beam, z is the direction of propagation of the oscillation, ρ is the material density, E is the Young's modulus, A is the cross-sectional area, T is the longitudinal tension, I is the second moment of area about the axis of bending, ω is the angular frequency of oscillation, q is the wavevector of the oscillation, and ϕ is the initial phase.

mode of the vibration one may neglect the tensile contribution and then determine the vibration frequency using the dispersion relation of Table 1.1, with the result

$$\omega_n = q_n^2\sqrt{\frac{E}{\rho}}\ t, \tag{1.4}$$

for a beam of rectangular cross-section (thickness t), and the solutions acquire an integer index n due to the imposition of boundary conditions.

Now, each mode may be considered as a simple harmonic oscillator with a single position coordinate and a single momentum coordinate, and with an effective spring constant and an effective mass. The spring constant may be calculated by calculating the static deflection due to a particular force distribution, and the effective mass follows from the known resonance frequency.

Two-dimensional and three-dimensional structures of interest include rectangular plates (such as graphene membranes), circular plates (such as microtoroidal resonators), and large cylinders and spheres (such as resonant-mass gravitational wave detectors). The appropriate wave equations can be determined, and the cor-

responding spatial mode solutions may be found in engineering textbooks [2].

1.2 Classical Mechanical Resonator

A harmonic oscillator is a system in which the restoring force is linearly proportional to the displacement, and which therefore has an oscillation frequency independent of the amplitude of motion. As noted above mechanical resonators can be described as harmonic oscillators. This picture is typically only valid where the amplitude of the vibrating element is not large.

1.2.1 Simple Harmonic Oscillator

Harmonic motion is ubiquitous in science and engineering. As noted, a particular vibration mode can be described as a single harmonic oscillator via continuum mechanics, which we now describe in detail in a particular case. Let us consider a thin doubly-clamped beam aligned such that the neutral axis of the beam is aligned along the z axis, with its ends clamped at $z = 0$ and $z = L$ (See Fig. 1.1). The

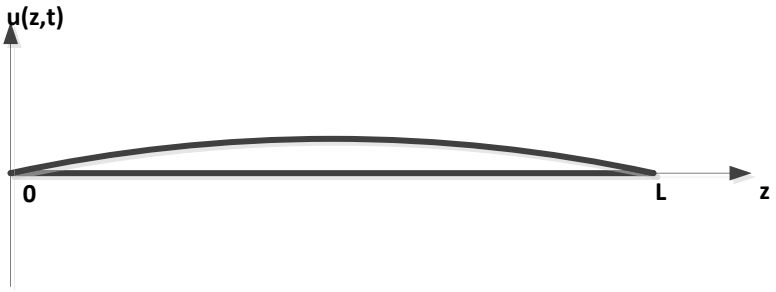

Figure 1.1: The coordinate system for transverse vibration of a doubly-clamped mechanical oscillator.

kinetic energy associated with the flexural motion of the beam is given by

$$K = \frac{1}{2}\int_V \rho \left[\frac{\partial u(z,t)}{\partial t}\right]^2 dV = \frac{1}{2}\rho A \dot{\mathcal{A}}^2 \int_0^L [u(z)]^2 dz = \eta_1 \frac{1}{2} M \dot{\mathcal{A}}^2, \qquad (1.5)$$

where V is the volume of the beam, ρ is its density, A is its cross-sectional area, $\mathcal{A}(t)$ is the time-dependent amplitude, and M is its mass. For the fundamental mode of the beam, $\eta_1 \equiv \frac{1}{L}\int_0^L [u(z)]^2 dz = 0.38$. The strain in the beam is assumed to be along the z axis and has amplitude $|x\frac{\partial^2 u(z,t)}{\partial z^2}|$. The potential energy associated with the strain in the beam is given in terms of a strain field $\epsilon(x,y,z,t)$ as

$$\begin{aligned} U &= \frac{1}{2}\int_V E[\epsilon(x,y,z,t)]^2 dV \\ &= \frac{E}{2}\int_{-t/2}^{+t/2} dx \int_{-\omega/2}^{+\omega/2} dy \int_0^L x^2 \left[\frac{\partial^2 u(z,t)}{\partial z^2}\right]^2 dz \\ &= \eta_1 \frac{1}{2} M\omega_m^2 \mathcal{A}^2, \end{aligned} \tag{1.6}$$

where E is the elastic modulus of the beam, w is the width of the beam and t is the thickness of the beam. Now we consider the representative position coordinate of the beam to be $x \equiv \mathcal{A}(t)$. The Lagrangian equation of motion corresponding to Eqs. (1.5) and (1.6) is then

$$\ddot{x} + \omega_m^2 x = 0. \tag{1.7}$$

This equation describes simple harmonic motion at the resonance frequency $\omega_m \equiv \sqrt{\frac{k}{m}}$ where m is the effective mass of the resonator and k is its effective spring constant. The corresponding classical Hamiltonian is

$$H = \frac{p^2}{2m} + \frac{1}{2}kx^2, \tag{1.8}$$

where p is a representative momentum coordinate. Such a description is generally valid, though the effective parameters depend on the system considered, the mode under consideration and the nature of the driving.

1.2.2 Damped Harmonic Resonator

In a damped harmonic oscillator a frictional force acts that is proportional to the oscillating velocity. The frictional force is present along with the restoring force

acting on the system for damped harmonic motion. When no driving forces are present, the equation of motion for a damped harmonic oscillator is

$$\ddot{x} + 2\zeta\omega_m\dot{x} + \omega_m^2 x = 0, \tag{1.9}$$

where $\omega_m = \sqrt{\frac{k}{m}}$ is the undamped angular frequency and $\zeta = \frac{c}{2\sqrt{mk}}$ is the damping ratio, with c being the viscous damping coefficient. A damped harmonic oscillator can be overdamped, critically damped or underdamped depending on the value of ζ. The *quality factor* expressed in terms of damping ratio is defined as

$$Q = \frac{1}{2\zeta}. \tag{1.10}$$

1.2.3 Mechanical Dissipation

The energy dissipation rate of a mechanical oscillator is given by

$$\gamma_m = \frac{\omega_m}{Q}. \tag{1.11}$$

There are several mechanism involved in the loss of mechanical energy. These include:

- Viscous damping $\longrightarrow$ caused by the friction/interaction with the surrounding gas atoms (Fig. 1.2) [3–5].
- Clamping losses $\longrightarrow$ caused by the radiation of elastic waves into the substrate through the supports of the oscillator [6–17].
- Fundamental anharmonicities $\longrightarrow$ caused by thermoelastic damping and phonon-phonon interactions [18–20].
- Materials-induced losses $\longrightarrow$ caused by the relaxation of intrinsic or extrinsic defect states in the bulk or surface of the resonator [21–25].

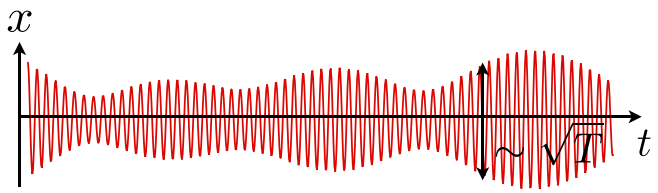

Figure 1.2: Position of an oscillator undergoing a Brownian motion (thermal fluctuations) with fluctuating amplitude and phase (figure reproduced from Ref. [26]).

The different dissipation mechanisms act independently and add up incoherently to the overall mechanical losses. The total quality factor Q_{total} is defined as

$$\frac{1}{Q_{\text{total}}} = \sum_i \frac{1}{Q_i}, \tag{1.12}$$

where Q_i denotes the mechanical quality factor associated with each dissipative mechanism.

1.2.4 Noise Spectra

A resonantly driven harmonic oscillator will have its trajectory $x(t)$ oscillating at the eigenfrequency ω_m. However, these oscillations show (see Fig. 1.3) randomly variable amplitude and phase due to the mechanical damping and fluctuating thermal Langevin force. Now such real-time measurements have been demonstrated in optomechanical systems [26]. For mechanical systems near the quantum limit, the undriven rather than the driven response is often considered. Analysis is often performed in the frequency domain, with the force and position noise spectra

$$S_F(\omega) = \frac{1}{2\pi}\int_{-\infty}^{\infty} dt e^{i\omega t} G_F(t), \tag{1.13}$$

$$S_x(\omega) = \frac{1}{2\pi}\int_{-\infty}^{\infty} dt e^{i\omega t} G_x(t), \tag{1.14}$$

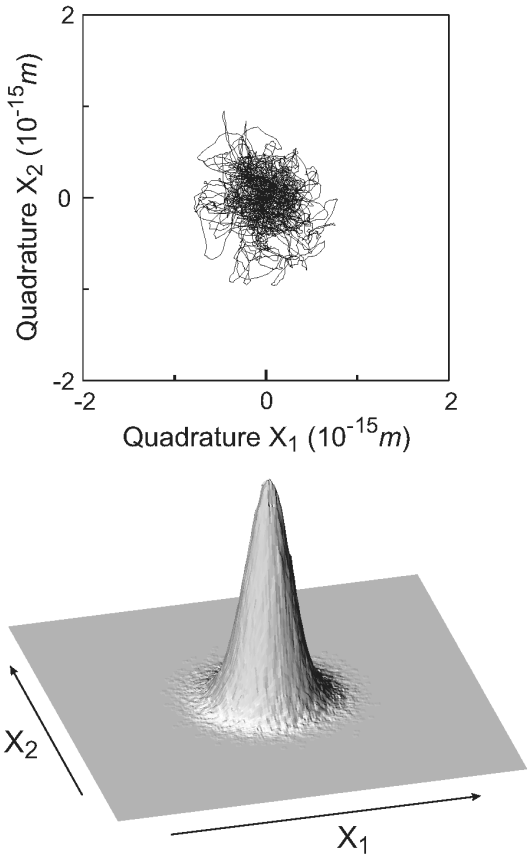

Figure 1.3: Thermal Brownian motion of a mechanical resonator in an optomechanical system, a trajectory of which is shown in the upper panel, leads to a probability distribution for the quadratures as shown in the lower panel. The two quadratures $x(t) = X_1(t)cos(\omega_m t) + X_2(t)sin(\omega_m t)$, are displayed in a frame rotating at the angular mechanical resonance frequency ω_m. The thermal Brownian motion cause the fluctuations (figure reproduced from Ref. [27]).

where G_F and G_x represent force and position auto-correlation functions, respectively. With thermal excitations as the source of noise, the classical force noise and position noise spectra can be written as

$$S_F(\omega) = 2m\gamma k_B T, \tag{1.15}$$

and

$$S_x(\omega) = \frac{k_B \gamma T}{2m\omega_m^2} \frac{1}{(\omega_m - \omega)^2 + (\gamma/2)^2}, \tag{1.16}$$

respectively. The force spectrum represent a so-called white noise process [27], having equal power at all frequencies.

1.3 Quantum Mechanical Resonator

1.3.1 Quantum Harmonic Oscillator

Next we consider the quantum approach to a macroscopic mechanical oscillator treated as a closed system (that is, no dissipation into an environment with many degree of freedom). We may consider the fundamental mode to be a quantum harmonic oscillator. The total energy operator or Hamiltonian for such a system is

$$\hat{H} = \frac{\hat{p}^2}{2m} + \frac{1}{2}m\omega_0^2\hat{x}^2, \tag{1.17}$$

where m is the particle's mass, ω_0 is the angular frequency of the oscillator, $\hat{x}$ is the position operator, and $\hat{p}$ is the momentum operator, given in a position-space representation by

$$\hat{p} = -i\hbar\frac{\partial}{\partial x}. \tag{1.18}$$

The position and momentum operator obey the commutation relation

$$[\hat{x}, \hat{p}] = i\hbar. \tag{1.19}$$

In Eq. (1.17) the first term in the Hamiltonian represents the kinetic energy of the particle, and the second term represents its potential energy. By solving Schrödinger's equation with the harmonic oscillator Hamiltonian, the energy eigenstates are found and they have the eigenvalues

$$E_n = \left(n + \frac{1}{2}\right)\hbar\omega_0, \tag{1.20}$$

with n indexing the eigenstates.

Alternatively, the so-called ladder operator method also allows us to extract the energy eigenvalues without directly solving the Schrödinger equation for a harmonic oscillator. Following this approach, we define the lowering operator $\hat{a}$ and (its adjoint) raising operator $\hat{a}^\dagger$ of a harmonic oscillator by

$$\hat{a} = \sqrt{\frac{m\omega_o}{2\hbar}}\hat{x} + i\frac{1}{\sqrt{2\hbar m\omega_o}}\hat{p}, \tag{1.21}$$

$$\hat{a}^\dagger = \sqrt{\frac{m\omega_o}{2\hbar}}\hat{x} - i\frac{1}{\sqrt{2\hbar m\omega_o}}\hat{p}. \tag{1.22}$$

The position and momentum operators may be written in terms of the raising and lowering operators as

$$\hat{x} = \sqrt{\tfrac{\hbar}{2}\tfrac{1}{m\omega}}(\hat{a}^\dagger + \hat{a}), \tag{1.23}$$

$$\hat{p} = i\sqrt{\tfrac{\hbar}{2}m\omega}(\hat{a}^\dagger - \hat{a}). \tag{1.24}$$

The commutation relations betweens the lowering and raising operators are $[\hat{a}, \hat{a}^\dagger] = 1$ and $[\hat{a}, \hat{a}] = [\hat{a}^\dagger, \hat{a}^\dagger] = 0$. The Hamiltonian can be written in terms of them as

$$\hat{H} = \hbar\omega_0\left(\hat{a}^\dagger\hat{a} + \frac{1}{2}\right). \tag{1.25}$$

The constant in Eq. (1.25) plays no role in the dynamics and is often dropped. The Hamiltonian of a quantum harmonic oscillator may be written in terms of dimensionless quadrature operators as

$$\hat{H} = \frac{\hbar\omega_0}{4}(\hat{X}^2 + \hat{P}^2), \tag{1.26}$$

where we have introduced the dimensionless position and momentum operators as

$$\hat{X} = \frac{\hat{x}}{\sqrt{\hbar/2m\omega_0}}, \tag{1.27}$$

$$\hat{P} = \frac{\hat{p}}{\sqrt{\hbar m\omega_0/2}}, \tag{1.28}$$

with the corresponding canonical commutation relation,

$$[\hat{X}, \hat{P}] = 2i. \tag{1.29}$$

1.3.2 Number State, Coherent State and Thermal State

The energy eigenvalues of a harmonic oscillator in Eq. (1.20) are associated with the energy eigenstates $|n\rangle$, called number or Fock states. They contain exactly n quanta (in our case, phonons).

An essential class of states of the harmonic oscillator are the coherent states. They are quasi-classical and they are the eigenstates of a driven harmonic oscillator. A coherent state can be given in terms of a number of state basis as,

$$|\alpha\rangle = e^{-|\alpha|^2/2} \sum_{n=0}^{\infty} \frac{\alpha^n}{\sqrt{n!}} |n\rangle. \tag{1.30}$$

Another important class of states are the so called thermal states. At temperature T the density matrix of a thermal state can be written as

$$\rho = (1 - e^{-\hbar\omega_0/k_B T}) \sum_{n=0}^{\infty} |n\rangle\langle n| e^{-n\hbar\omega_0/k_B T}. \tag{1.31}$$

The expected number of phonons in a thermal state is

$$\bar{n} \equiv \langle \hat{n} \rangle = \frac{1}{e^{-\hbar\omega_m/k_B T} - 1} \approx \frac{k_B T}{\hbar\omega_m} (k_B T \gg \hbar\omega_m). \tag{1.32}$$

The ground state is the lowest energy state corresponding to $\bar{n} = 0$. The necessary condition for a mode to be in its quantum ground state in a cryogenic environment is that

$$\hbar\omega_m \gg k_B T. \tag{1.33}$$

1.4 Cavity Optomechanics

1.4.1 Optical Cavities

To model an optical cavity, we consider a Fabry-Pérot resonator consisting of two highly reflective mirrors, separated by a distance L. The angular frequencies of the resonances of the cavity are $\omega_0 = n\pi\frac{c}{L}$, where n is an integer mode number. The free spectral range (FSR) of the cavity, meaning the frequency spacing between adjacent resonant modes, will be

$$\Delta\omega_{FSR} = \pi\frac{c}{L}. \tag{1.34}$$

The quality factor of a optical cavity is given by

$$Q = \omega_0\tau, \tag{1.35}$$

where ω_0 is the frequency of a single optical mode, and $\tau = \kappa^{-1}$ is the photon lifetime in the cavity, with the cavity intensity decay rate denoted by κ. Note that the cavity decay rate has two parts consists of the (useful) input/output coupling κ_e and the internal losses κ_i, as

$$\kappa = \kappa_e + \kappa_i, \tag{1.36}$$

A quantum mechanical description of a cavity that is coupled to a continuum of external field modes can be described either via master equations or via a framework known as quantum input-output theory [28, 29]. By applying the input-output theory of open quantum systems, the output field from the Fabry-Pérot resonator is given by

$$\hat{a}_{out} = \hat{a}_{in} - \sqrt{\kappa_e}\hat{a}, \tag{1.37}$$

where $\hat{a}$ is the intracavity field and $\hat{a}_{in}$ refers to the input field. For the optical res-

onator we assume two completely uncorrelated baths, corresponding to the extrinsic and intrinsic decay channels. Although an input-output boundary condition may also be defined for the intrinsic optical bath and the mechanical bath, by definition these baths are unmonitored, and the input and output fields are a mathematical construct that allows the treatment of dissipation, but are not physically meaningful themselves. The equation of motion for the intracavity field resonator is

$$\dot{\hat{a}} = -\frac{\kappa}{2}\hat{a} + i\Delta\hat{a} + \sqrt{\kappa_e}\hat{a}_{in} + \sqrt{\kappa_i}\hat{f}_{in}, \tag{1.38}$$

in a frame rotating at a driving frequency $\omega_d = \omega_c + \Delta$, where ω_c is the cavity frequency. Note that $\hat{f}_{in}$ represents the input noise fluctuation in Eq. (1.38). We can solve Eq. (1.38) by assuming $\langle \hat{f}_{in} \rangle = 0$, and we find that

$$\langle \hat{a} \rangle_{ss} = \frac{\sqrt{\kappa_e}\langle \hat{a}_{in} \rangle}{\frac{\kappa}{2} - i\Delta}. \tag{1.39}$$

This Eq. (1.39) can be used to calculate the steady-state cavity population (that is, the average number of photons circulating inside the cavity) as

$$\bar{n}_{cav} = \langle \hat{a}^\dagger \hat{a} \rangle = \frac{\kappa_e}{\Delta^2 + (\kappa/2)^2} \frac{P}{\hbar\omega_L}, \tag{1.40}$$

where P is the input power driven into the cavity. By using Eqs. (1.37) and (1.39) the reflection amplitude of a single-sided cavity coupled in reflection may be given by,

$$R = \frac{\langle \hat{a}_{out} \rangle}{\langle \hat{a}_{in} \rangle} = \frac{(\kappa_i - \kappa_e)/2 - i\Delta}{(\kappa_i + \kappa_e)/2 - i\Delta}. \tag{1.41}$$

Several regimes, neglecting the detuning, can be obtained from this expression:

- Over-coupling $\longrightarrow$ For $\mid R \mid^2 \approx 1$ the pump photons come out from the cavity without having been absorbed or lost at the second mirror. This case corresponds to external coupling being much bigger than the cavity losses ($\kappa_e > \kappa_i$).

- Critical Coupling $\longrightarrow$ For $\mid R \mid^2 = 0$ the input energy is either fully dissipated in the resonator and fully transmitted through the second mirror. The external coupling will be equal to the cavity intrinsic losses ($\kappa_e = \kappa_i$).

- Undercoupling $\longrightarrow$ Here cavity losses will be much bigger than the external coupling ($\kappa_e << \kappa_i$).

1.4.2 Optomechanical Coupling

The canonical model of a cavity optomechanical system is shown in Fig. 1.4. The Fabry-Pérot cavity shown has an optical resonance frequency ω_c, and one end mirror of the cavity is mechanically compliant (shown here as a massive mirror mounted on a spring). The mechanical oscillator behaves as a damped harmonic oscillator. The

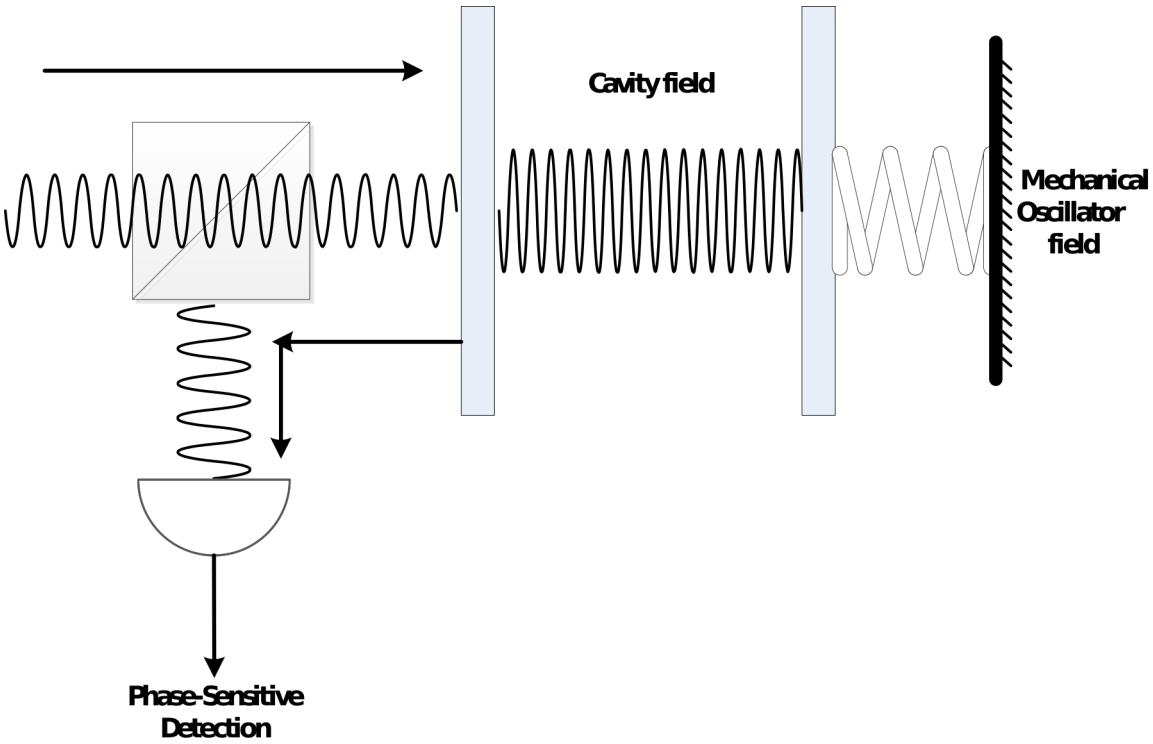

Figure 1.4: A canonical cavity optomechanical system, consisting of a Fabry-Pérot cavity with a moving end-mirror. The intracavity optical field ($\hat{a}$) couples to the mechanical oscillator ($\hat{b}$). This produces phase modulation of an optical cavity drive, and phase-sensitive detection of the cavity refection may be used to measure the mechanical displacement.

Hamiltonian for such a system, in the absence of any optomechanical interaction is

$$\hat{H} = \hbar\omega_c \hat{a}^\dagger \hat{a} + \hbar\omega_m \hat{b}^\dagger \hat{b}, \tag{1.42}$$

where $\hat{b}$ and $\hat{b}^\dagger$ represent the mechanical oscillator's lowering and raising operators, respectively. Now the instantaneous cavity length L is related to the equilibrium cavity length L_0 by $L = L_0 + x$, such that x is the displacement of the mirror. The cavity resonance frequency is then explicitly position-dependent as,

$$\omega_c(x) = \omega_c + \frac{\omega_c}{L_0} x. \tag{1.43}$$

Substituting Eq. (1.43) into Eq. (1.42) then leads to

$$\hat{H} = \hbar\omega_c \hat{a}^\dagger \hat{a} + \hbar\omega_m \hat{b}^\dagger b - \hbar \frac{g_0}{x_{zp}} \hat{a}^\dagger \hat{a} \hat{x}, \tag{1.44}$$

where we identify the single-photon optomechanical coupling rate as

$$g_0 = \omega_c \frac{\Delta x_{zp}}{L_0}, \tag{1.45}$$

where Δx_{zp} is the width of the quantum ground state fluctuations of the mechanical oscillator. Writing the position operator in terms of a mechanical lowering and raising operator, we have

$$\hat{H} = \hbar\omega_c \hat{a}^\dagger \hat{a} + \hbar\omega_m \hat{b}^\dagger b - \hbar g_0 \hat{a}^\dagger \hat{a} (\hat{b} + \hat{b}^\dagger). \tag{1.46}$$

While we explicitly considered a simple Fabry-Pérot cavity here, the Hamiltonian of Eq. (1.46) is much more general. It applies to any system where the motion of a mechanical oscillator shifts the resonance frequency of an electromagnetic cavity. Now moving into an interaction picture for both the optical and mechanical

resonator Eq. (1.46) becomes

$$\hat{H} = \hbar g_0 \hat{a}^\dagger \hat{a}(\hat{b}e^{-i\omega_m t} + \hat{b}^\dagger e^{i\omega_m t}). \tag{1.47}$$

Now, changing the cavity driving conditions we can easily change the effective optomechanical coupling [30], if we assume resolved-sideband ($\omega_m \gg \kappa$). This is most easily understood by considering the interaction in the frequency domain, as shown in Fig. 1.5.

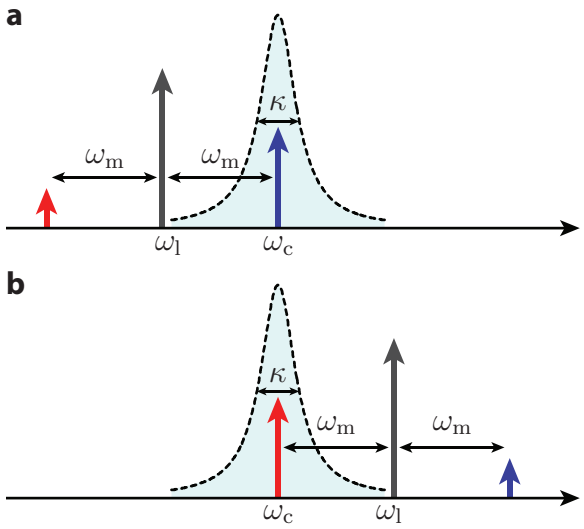

Figure 1.5: Linearised sideband-resolved optomechanics represented in the frequency domain. The optomechanical interaction scatters a coherent drive tone to produce red and blue sidebands corresponding to phonon absorption and emission, respectively. In the sideband-resolved regime, the modified density of states provided by the optical cavity may be used to enhance one or the other scattering process. For red-detuned driving (a) this results in an effective beam-splitter-like Hamiltonian which may be used for cooling or state transfer. For blue-detuned driving (b) the effective Hamiltonian has the form of two-mode squeezing, useful for amplification of the mechanical motion or the generation of non-classical optomechanical states (figure reproduced from Ref. [33]).

Suppose the cavity mode is driven at a frequency ω_1. In the experimentally relevant weak coupling regime, where the single-photon coupling rate g_0 is less than the cavity decay rate κ, the optomechanical interaction will generate optical sidebands at the frequencies $\omega_1 \pm \omega_m$. The upper sideband at $\omega_1 + \omega_m$, is generated

by the interaction term $\hat{a}^\dagger\hat{b}$ and represents the up-conversion of a drive photon accompanied by the absorption of a phonon from the mechanical resonator. On the other hand, the lower sideband at $\omega_1 - \omega_m$, is generated by the $\hat{a}^\dagger\hat{b}^\dagger$ interaction term and corresponds to the down-conversion of drive photons accompanied by the emission of a phonon.

Now, if the drive is blue-detuned from the cavity ($\omega_1 = \omega_c + \omega_m$), the red sideband is resonantly enhanced, as shown in Fig. 1.5(b), and one can derive a linearized interaction in a rotating wave approximation

$$\hat{H}^b_{eff} = \hbar g(\hat{a}\hat{b} + \hat{a}^\dagger\hat{b}^\dagger), \tag{1.48}$$

where $g = \alpha g_0$ is the effective optomechanical coupling strength, with α denoting the steady state amplitude of the coherent drive field. This interaction, which has the form of two-mode squeezing, allows one to amplify the mechanical motion, as the process of phonon emission rather than absorption is now dominant. Conversely, if the drive is placed at a lower frequency (red-detuned), then the blue sideband is resonantly enhanced ($\omega_c = \omega_c - \omega_m$), as shown in Fig. 1.5(a), the effective Hamiltonian can be written as

$$\hat{H}^r_{eff} = \hbar g(\hat{a}^\dagger\hat{b} + \hat{a}\hat{b}^\dagger), \tag{1.49}$$

where g is the effective optomechanical coupling strength as above. If we consider the two-tone driving [31, 32], simultaneously exciting the red and blue transitions [33], the effective Hamiltonian is simply the sum of Eqs. (1.48) and (1.49),

$$\hat{H}^{br}_{eff} = \hbar g(\hat{a} + \hat{a}^\dagger)(\hat{b}e^{-i\phi} + \hat{b}^\dagger e^{+i\phi}), \tag{1.50}$$

where ϕ is the relative phase of two driving fields. This Hamiltonian commutes with a mechanical quadrature operator, and thus implements a quantum nondemolition measurement of such a quadrature. Which mechanical quadrature is measured, is determined by the choice of ϕ, the cavity driving tones.

1.4.3 Optomechanical Equation of Motion

A theoretical treatment of the cavity optomechanical system starts from the Heisenberg equations of motion. While the optomechanical Hamiltonian given in Eq. (1.46) describes the internal dynamics of the system, it does not incorporate the effects of damping and noise due to the surrounding environment. Such effects can be introduced via the standard input-output formalism for open quantum systems [4, 5], which is briery summarised in Section 1.4.1. This leads to the Heisenberg-Langevin equations with the radiation pressure interaction for the photon and phonon annihilation operators:

$$\frac{d}{dt}\hat{a} = -i(\omega_c + \tfrac{\kappa}{2})\hat{a} - ig_0(\hat{b} + \hat{b}^\dagger)\hat{a} + \sqrt{\kappa_e}\hat{a}_{in} + \sqrt{\kappa_i}\hat{a}_i, \tag{1.51}$$

$$\frac{d}{dt}\hat{b} = -i(\omega_m + \tfrac{\gamma}{2})\hat{b} - ig\hat{a}^\dagger\hat{a} + \sqrt{\gamma}\hat{b}_{in}, \tag{1.52}$$

where γ and $\kappa = \kappa_e + \kappa_i$ are the decay rates of the mechanical and optical oscillators, respectively. The noise operator $\hat{b}_{in}$ arises from the coupling between the mechanical oscillator and its surrounding environment.

The coupling of the optical cavity to its environment has been separated into two channels: the extrinsic channel, with coupling rate κ_e and noise operator $\hat{a}_{in}$, and the intrinsic channel, with coupling rate κ_i and noise operator $\hat{a}_i$. The extrinsic channel is the specific mode via which the cavity is probed, while the intrinsic channel represents all other environmental loss channels that go unmeasured (e.g., radiation of energy due to scattering, material absorption inside the cavity, etc.). Both optical noise operators are assumed Markovian and so obey the same type of commutation relation as $\hat{b}_{in}$. The output field in the external channel is given by the input-output boundary condition described in Eq. (1.37). While $\hat{b}_{in}$ and $\hat{a}_i$ are zero-mean, $\hat{a}_{in}$ typically consists of both a classical tone (technically, a coherent state) at frequency ω_1 in addition to stochastic noise. We may explicitly factor out both the harmonic time dependence of the operator as well as the classical amplitude α_{in} by making the substitution $\hat{a}_{in} = (\alpha_{in} + \hat{a}_{in})e^{-i\omega_1 t}$, and this classical tone is

incorporated into the effective optomechanical coupling rate. As the optical drive frequency is much faster than the decay rates of the system and the mechanical frequency, it is convenient to move into a frame rotating at the drive frequency, focusing only on the slowly varying dynamics. This is accomplished by making a unitary transformation, that leads to the equations of motion as

$$\frac{d}{dt}\hat{a} = -(i\delta + \tfrac{\kappa}{2})\hat{a} - ig_0(\hat{b} + \hat{b}^\dagger)\hat{a} + \sqrt{\kappa_e}(\alpha_{in} + \hat{a}_{in}) + \sqrt{\kappa_i}\hat{a}_i, \tag{1.53}$$

$$\frac{d}{dt}\hat{b} = -i(\omega_m + \tfrac{\gamma}{2})\hat{b} - ig_0\hat{a}^\dagger\hat{a} + \sqrt{\gamma}\hat{b}_{in}, \tag{1.54}$$

where $\delta = \omega_c - \omega_1$ is the detuning between cavity and the drive. Though we have made no assumptions so far as to the nature of the environmental noise, the mechanical bath is typically taken to be in thermal equilibrium at temperature T, such that the mechanical noise operator obeys the following correlation relations

$$\langle \hat{b}_{in}^\dagger(t)\hat{b}_{in}(t')\rangle = \bar{n}\delta(t - t'), \tag{1.55}$$

$$\langle \hat{b}_{in}(t)\hat{b}_{in}^\dagger(t')\rangle = (\bar{n} + 1)\delta(t - t'), \tag{1.56}$$

where $\bar{n} = (e^{\hbar\omega_m/k_BT} - 1)^{-1}$ is the Bose factor giving the occupancy of the mechanical bath in thermal equilibrium at temperature T, and all other one- and two-time correlation functions of $\hat{b}_{in}$ or $\hat{b}_{in}^\dagger$ are zero. The intrinsic optical bath is usually taken to be a thermal bath as well, but in the case of optical systems at room temperature the frequency is large enough ($\hbar\omega_c, \hbar\omega_1 \gg k_BT$) that the bath is well-approximated as being zero-temperature (i.e., vacuum). Thus, the corresponding noise correlation functions are

$$\langle \hat{a}_i^\dagger(t)\hat{a}_i(t')\rangle = 0, \tag{1.57}$$

$$\langle \hat{a}_i(t)\hat{a}_i^\dagger(t')\rangle = \delta(t - t'), \tag{1.58}$$

where, as in the case of the mechanical noise, all other two-time correlations vanish. The optical noise on the extrinsic channel, a_{in}, is typically also assumed to

be vacuum noise, and thus has the same type of correlation functions shown in Eqs. (1.57) and (1.58) (note that $\hat{a}_{in}$ and $\hat{a}_i$ belong to independent baths and are thus uncorrelated with each other). It is also possible for $\hat{a}_{in}$ to have additional noise due to technical noise on the input drive.

1.5 Master Equation

An alternative approach to describing the evolution of a quantum system rather than in terms of its observables is to specify its evolution in terms of its density matrix (an operator describing its state). Equations describing the evolution of a systems density matrix are often referred to as master equation [34]. Here, we briefly outline the description of a standard form of Markovian master equation called the Lindblad master equation.

Let us consider, a quantum system S, coupled to an environment (or bath) B. The state of the subsystem S is changing as a consequence of its internal dynamics and the interaction with its surrounding degree of freedom. If H_S is the Hilbert space of the system and H_B is the Hilbert space of the environment, then the Hilbert space of the total system is $H = H_S \otimes H_B$. We assume at the initial time t_0, the uncorrelated density matrix

$$\rho(t_0) = \rho_S(t_0) \otimes \rho_B, \tag{1.59}$$

where $\rho_S(t_0)$ is the initial state of the reduced system S and ρ_B represents some equilibrium state of the bath. Assuming the unitary evolution of the reduced density operator of the system as

$$\rho_S(t) = \mathrm{Tr}_B \rho(t) = \mathrm{Tr}_B\{U(t,t_0)\rho(t_0)U^\dagger(t,t_0)\}, \tag{1.60}$$

where $U(t,t_0)$ is the unitary evolution operator of the total system. In general, it is

not possible to calculate the exact dynamics according to Eq. (1.60), and we must approximate to make the problem tractable. There are two common approaches to calculate the exact dynamics of the reduced density operator of a system. They are based on the Liouville-von Neumann equation and the use of path integrals. The Liouville-von Neumann equation approach gives us a time-local, first-order differential equation for the reduced density operator of the system, known as master equation.

Assuming that the system Hamiltonian is $\hat{H}_S$, and the Hamiltonian for the environment is $\hat{H}_B$, and we let the interaction between the system and bath be denoted by $\hat{H}_I$. Now by moving to an interaction picture with respect to $\hat{H}_S + \hat{H}_B$, the time-evolution of the density matrix is described by the Liouville-von Neumann equation:

$$\frac{d}{dt}\rho(t) = -\frac{i}{\hbar}[\hat{H}_I(t), \rho(t)]. \tag{1.61}$$

A master equation can also be derived in Lindbad form [35] for the reduced density operator

$$\frac{d}{dt}\rho_s(t) = -\frac{i}{\hbar}[\hat{H}'_S, \rho_s(t)] + \frac{1}{2}\sum_k \gamma_k[2L_k\rho_s(t)L_k^\dagger - L_k^\dagger L_k\rho_s(t) - \rho_s(t)L_k^\dagger L_k], \tag{1.62}$$

where ρ_s is the reduced density matrix of the system alone, L_k are called Lindblad operators describing the effect of the environmental degrees of freedom on the system, γ_k is the decoherence rates, and $\hat{H}'_S$ is the reduced system Hamiltonian. If the Lindblad operators are all Hermitian, then Eq. (1.62) can be re-written as

$$\frac{d}{dt}\rho_s(t) = -\frac{i}{\hbar}[\hat{H}'_S, \rho_s(t)] + \frac{1}{2}\sum_k \gamma_k[\hat{L}_k, [\hat{L}_k, \rho_s(t)]]. \tag{1.63}$$

For a single harmonic oscillator system the quantum optical master equation, sub-

ject to linear damping into a thermal environment, Eq. (1.62) becomes

$$\frac{d}{dt}\rho_s = -i[\omega_m \hat{a}^\dagger \hat{a}, \rho_s] + \gamma(\bar{n}+1)(\hat{a}\rho_s\hat{a}^\dagger - \frac{1}{2}\hat{a}^\dagger\hat{a}\rho_s - \frac{1}{2}\hat{a}^\dagger\hat{a}\rho_s) + \gamma\bar{n}(\hat{a}^\dagger\rho_s\hat{a} - \frac{1}{2}\hat{a}\hat{a}^\dagger\rho_s - \frac{1}{2}\hat{a}\hat{a}^\dagger\rho_s), \tag{1.64}$$

where $\bar{n}$ is the thermal occupation of the environment, given by a Bose-Einstein distribution, and γ is the damping rate of the harmonic oscillator.

Chapter 2

Dissipative State Preparation in Cavity Quantum Optomechanics

From a Lindblad master equation we can readily determine the steady states generated with a quadratic Hamiltonian and linear dissipation. We now explore these possibilities with one and two oscillator modes. Dissipative preparation of quantum squeezed states of macroscopic mechanical oscillators has recently been demonstrated experimentally.

2.1 Single Harmonic Oscillator in Thermal Equilibrium

A simple case is a single harmonic oscillator in a thermal environment, the corresponding Lindbard master equation of a single harmonic oscillator defined in a frame rotating at the oscillator resonance frequency is then

$$\dot{\rho} = \gamma(\bar{n}+1)\mathcal{D}[\hat{a}]\rho + \gamma\bar{n}\mathcal{D}[\hat{a}^\dagger]\rho, \tag{2.1}$$

where $\bar{n}$ is the thermal occupation of the environment and $\mathcal{D}[\hat{a}]\rho$ is the the cavity dissipative superoperator. The dissipative superoperator can be defined as

$$\mathcal{D}[\hat{O}]\rho = \hat{O}\rho\hat{O}^\dagger - \frac{1}{2}\rho\hat{O}^\dagger\hat{O} - \frac{1}{2}\hat{O}^\dagger\hat{O}\rho. \tag{2.2}$$

One can readily obtain the Heisenberg equations of motion for the first and second moments of system observables using $\frac{d}{dt}\langle\hat{A}\rangle = \mathrm{Tr}(\hat{A}\dot{\rho})$ as

$$\frac{d}{dt}\langle\hat{a}^2\rangle = -\gamma\langle\hat{a}^2\rangle, \tag{2.3a}$$
$$\frac{d}{dt}\langle\hat{a}^{\dagger 2}\rangle = -\gamma\langle\hat{a}^{\dagger 2}\rangle, \tag{2.3b}$$
$$\frac{d}{dt}\langle\hat{a}^\dagger\hat{a}\rangle = -\gamma\langle\hat{a}^\dagger\hat{a}\rangle + \gamma\bar{n}, \tag{2.3c}$$
$$\frac{d}{dt}\langle\hat{a}\hat{a}^\dagger\rangle = -\gamma\langle\hat{a}\hat{a}^\dagger\rangle + \gamma(\bar{n}+1). \tag{2.3d}$$

At steady state, expectation values can be calculated from the above equations as

$$\langle\hat{a}^2\rangle = 0, \langle\hat{a}^{\dagger 2}\rangle = 0, \langle\hat{a}^\dagger\hat{a}\rangle = \bar{n}, \langle\hat{a}\hat{a}^\dagger\rangle = 1+\bar{n}. \tag{2.4}$$

That is, the steady state has $\bar{n}$ thermal quanta but no coherent amplitude. We can look at this steady-state in terms of dimensionless oscillator quadratures

$$\hat{X} = \tfrac{1}{\sqrt{2}}(\hat{a}+\hat{a}^\dagger), \tag{2.5}$$
$$\hat{P} = -\tfrac{i}{\sqrt{2}}(\hat{a}-\hat{a}^\dagger). \tag{2.6}$$

In terms of these oscillator quadratures, the symmetrically-ordered covariance matrix can be written as

$$V = \begin{bmatrix} \langle X^2\rangle & \frac{\langle\hat{X}\hat{P}+\hat{P}\hat{X}\rangle}{2} \\ \frac{\langle\hat{P}\hat{X}+\hat{X}\hat{P}\rangle}{2} & \langle P^2\rangle \end{bmatrix}. \tag{2.7}$$

In the steady state we obtain the covariance matrix for single oscillator as

$$V = \begin{bmatrix} \bar{n} + \frac{1}{2} & 0 \\ 0 & \bar{n} + \frac{1}{2} \end{bmatrix}. \tag{2.8}$$

That is, each quadrature observable possesses thermal and quantum zero-point fluctuations.

The purity of a quantum state is a scalar quantified as

$$\mu = \mathrm{Tr}(\rho^2). \tag{2.9}$$

It gives, on a scale of 0 to 1, an indication of the extent of our knowledge of the state of the system under consideration; a purity of 1 corresponds to the maximal knowledge allowed by quantum mechanics. For Gaussian states, the purity may be evaluated in terms of the covariance matrix as [36]

$$\mu = \frac{1}{2^n \sqrt{\mathrm{Det} V}}, \tag{2.10}$$

where n denotes the number of the modes. If μ is 1, it corresponds to a pure state whereas $\mu < 1$ is corresponds to a mixed state. Now the purity found for the single harmonic oscillator in a thermal state is

$$\mu = \frac{1}{2\bar{n} + 1}. \tag{2.11}$$

That is, the system will be in a pure state if the thermal occupation of the bath is at zero, but there is increasing statistical uncertainty over the state of the system as the temperature is increased.

2.2 Two Harmonic Oscillators in Thermal Equilibrium

Next we consider two independent harmonic oscillators (a and b) coupled to independent thermal Markovian environments. Again, the master equation is specified in a frame rotating at both oscillators resonance frequencies. It is

$$\dot{\rho} = \gamma_a(\bar{n}_a + 1)\mathcal{D}[\hat{a}]\rho + \gamma_a\bar{n}_a\mathcal{D}[\hat{a}^\dagger]\rho + \gamma_b(\bar{n}_b + 1)\mathcal{D}[\hat{b}]\rho + \gamma_b\bar{n}_b\mathcal{D}[\hat{b}^\dagger]\rho, \tag{2.12}$$

where γ_a and γ_b are the damping rates, and $\bar{n}_a$ and $\bar{n}_b$ are the thermal occupations of the baths.

For two harmonic oscillators the Heisenberg equations of motion for second moments of system observables are found as,

$$\frac{d}{dt}\langle\hat{a}^2\rangle = -\gamma_a\langle\hat{a}^2\rangle, \tag{2.13a}$$
$$\frac{d}{dt}\langle\hat{a}^{\dagger 2}\rangle = -\gamma_a\langle\hat{a}^{\dagger 2}\rangle, \tag{2.13b}$$
$$\frac{d}{dt}\langle\hat{b}^2\rangle = -\gamma_b\langle\hat{b}^2\rangle, \tag{2.13c}$$
$$\frac{d}{dt}\langle\hat{b}^{\dagger 2}\rangle = -\gamma_b\langle\hat{b}^{\dagger 2}\rangle, \tag{2.13d}$$
$$\frac{d}{dt}\langle\hat{a}^\dagger\hat{a}\rangle = -\gamma_a\langle\hat{a}^\dagger\hat{a}\rangle + \gamma_a\bar{n}_a, \tag{2.13e}$$
$$\frac{d}{dt}\langle\hat{a}\hat{a}^\dagger\rangle = -\gamma_a\langle\hat{a}^\dagger\hat{a}\rangle + \gamma_a(\bar{n}_a + 1), \tag{2.13f}$$
$$\frac{d}{dt}\langle\hat{b}^\dagger\hat{b}\rangle = -\gamma_b\langle\hat{b}^\dagger\hat{b}\rangle + \gamma_b\bar{n}_b, \tag{2.13g}$$
$$\frac{d}{dt}\langle\hat{b}\hat{b}^\dagger\rangle = -\gamma_b\langle\hat{b}\hat{b}^\dagger\rangle + \gamma_b(\bar{n}_b + 1), \tag{2.13h}$$
$$\frac{d}{dt}\langle\hat{a}\hat{b}\rangle = -\left(\frac{\gamma_a + \gamma_b}{2}\right)\langle\hat{a}\hat{b}\rangle, \tag{2.13i}$$
$$\frac{d}{dt}\langle\hat{a}^\dagger\hat{b}^\dagger\rangle = -\left(\frac{\gamma_a + \gamma_b}{2}\right)\langle\hat{a}^\dagger\hat{b}^\dagger\rangle, \tag{2.13j}$$
$$\frac{d}{dt}\langle\hat{a}^\dagger\hat{b}\rangle = -\left(\frac{\gamma_a + \gamma_b}{2}\right)\langle\hat{a}^\dagger\hat{b}\rangle, \tag{2.13k}$$
$$\frac{d}{dt}\langle\hat{a}\hat{b}^\dagger\rangle = -\left(\frac{\gamma_a + \gamma_b}{2}\right)\langle\hat{a}\hat{b}^\dagger\rangle. \tag{2.13l}$$

At steady state, expectation values can be calculated from the above equations as

$$\begin{gathered}\langle\hat{a}^2\rangle = 0, \langle\hat{a}^{\dagger 2}\rangle = 0, \langle\hat{b}^2\rangle = 0, \langle\hat{b}^{\dagger 2}\rangle = 0, \\ \langle\hat{a}^\dagger\hat{a}\rangle = \bar{n}_a, \langle\hat{a}\hat{a}^\dagger\rangle = 1 + \bar{n}_a, \langle\hat{b}^\dagger\hat{b}\rangle = \bar{n}_b, \langle\hat{b}\hat{b}^\dagger\rangle = 1 + \bar{n}_b, \\ \langle\hat{a}\hat{b}\rangle = 0, \langle\hat{a}^\dagger\hat{b}^\dagger\rangle = 0, \langle\hat{a}^\dagger\hat{b}\rangle = 0, \langle\hat{a}\hat{b}^\dagger\rangle = 0.\end{gathered} \tag{2.14}$$

The steady-state covariance matrix, in the order of oscillator quadrature operators ($\hat{X}_a$, $\hat{P}_a$, $\hat{X}_b$, $\hat{P}_b$) is

$$V = \begin{bmatrix} \langle\hat{X}_a^2\rangle & \frac{\langle\hat{X}_a\hat{P}_a+\hat{P}_a\hat{X}_a\rangle}{2} & \langle\hat{X}_a\hat{X}_b\rangle & \langle\hat{X}_a\hat{P}_b\rangle \\ \frac{\langle\hat{P}_a\hat{X}_a+\hat{X}_a\hat{P}_a\rangle}{2} & \langle\hat{P}_a^2\rangle & \langle\hat{P}_a\hat{X}_b\rangle & \langle\hat{P}_a\hat{P}_b\rangle \\ \langle\hat{X}_b\hat{X}_a\rangle & \langle\hat{X}_b\hat{P}_a\rangle & \langle\hat{X}_b^2\rangle & \frac{\langle\hat{X}_b\hat{P}_b+\hat{P}_b\hat{X}_b\rangle}{2} \\ \langle\hat{P}_b\hat{X}_a\rangle & \langle\hat{P}_b\hat{P}_a\rangle & \frac{\langle\hat{P}_b\hat{X}_b+\hat{X}_b\hat{P}_b\rangle}{2} & \langle\hat{P}_b^2\rangle \end{bmatrix}. \tag{2.15}$$

The covariance matrix calculated from two oscillators is defined by,

$$V = \begin{bmatrix} \bar{n}_a + \frac{1}{2} & 0 & 0 & 0 \\ 0 & \bar{n}_a + \frac{1}{2} & 0 & 0 \\ 0 & 0 & \bar{n}_b + \frac{1}{2} & 0 \\ 0 & 0 & 0 & \bar{n}_b + \frac{1}{2} \end{bmatrix}. \tag{2.16}$$

Like the single harmonic oscillator system, it is clear from Eq. (2.16) that for a zero-temperature bath (that is $\bar{n}_a = 0$, $\bar{n}_b = 0$), the system will be in a pure state. Each harmonic oscillator is subject to independent thermal and quantum zero-point fluctuations.

2.3 Cooling a Single Harmonic Oscillator

Here we augment the intrinsic coupling to a thermal bath with an engineered coupling to a zero-temperature bath. This constitutes a minimal model for the description of dynamical back-action cooling in cavity optomechanics. Here the master

equation can written as

$$\dot{\rho} = \gamma(\bar{n}+1)\mathcal{D}[\hat{a}]\rho + \gamma\bar{n}\mathcal{D}[\hat{a}^\dagger]\rho + \Gamma\mathcal{D}[\hat{a}]\rho, \tag{2.17}$$

where Γ represents an engineered cooling rate into an auxiliary zero-temperature bath. In the cavity optomechanics context, this is a description of the electromagnetic cavity mode after the cavity has been adiabatically eliminated, and $\Gamma = 4g^2/\kappa$, where g is the optomechanical coupling rate and κ is the cavity decay rate. Here the equations of motion for second moments of system observables are calculated as

$$\frac{d}{dt}\langle\hat{a}^2\rangle = -(\gamma+\Gamma)\langle\hat{a}^2\rangle, \tag{2.18a}$$
$$\frac{d}{dt}\langle\hat{a}^{\dagger^2}\rangle = -(\gamma+\Gamma)\langle\hat{a}^{\dagger^2}\rangle, \tag{2.18b}$$
$$\frac{d}{dt}\langle\hat{a}^\dagger\hat{a}\rangle = -(\gamma+\Gamma)\langle\hat{a}^\dagger\hat{a}\rangle + \gamma\bar{n}, \tag{2.18c}$$
$$\frac{d}{dt}\langle\hat{a}\hat{a}^\dagger\rangle = -(\gamma+\Gamma)\langle\hat{a}\hat{a}^\dagger\rangle + \gamma(\bar{n}+1). \tag{2.18d}$$

The expectation values calculated at the steady-state

$$\langle\hat{a}^2\rangle = 0, \langle\hat{a}^{\dagger^2}\rangle = 0, \langle\hat{a}^\dagger\hat{a}\rangle = \frac{\gamma}{\gamma+\Gamma}\bar{n}, \langle\hat{a}\hat{a}^\dagger\rangle = 1 + \frac{\gamma}{\gamma+\Gamma}\bar{n}. \tag{2.19}$$

The covariance matrix found as

$$V = \begin{bmatrix} \frac{\gamma}{\gamma+\Gamma}\bar{n} + \frac{1}{2} & 0 \\ 0 & \frac{\gamma}{\gamma+\Gamma}\bar{n} + \frac{1}{2} \end{bmatrix}. \tag{2.20}$$

Clearly, for $\Gamma \ll \gamma$ the quadratures are subject to their full thermal and quantum zero-point fluctuations. For $\Gamma \gg \gamma$, the thermal fluctuations are largely attenuated but the zero-point fluctuations remain. This describes the cooling of an oscillator to its quantum ground state, as has been experimentally demonstrated [37].

Fig. 2.1 represents that the gradual change of expectation value $\langle\hat{a}\hat{a}^\dagger\rangle = \langle\hat{a}^\dagger\hat{a}\rangle + 1$

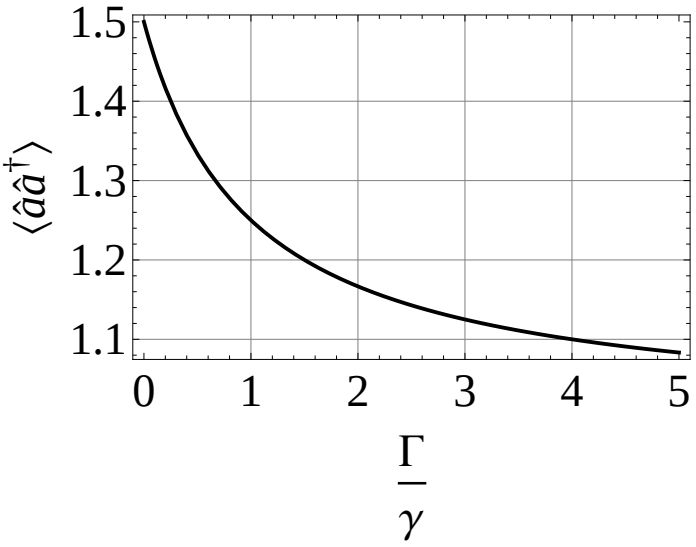

Figure 2.1: Steady-state occupation of harmonic oscillator plus one, $\langle \hat{a}\hat{a}^\dagger \rangle$, as a function of the ratio of damping rate into a zero-temperature environment to the damping rate into a finite-temperature environment.

with the ratio of cooling rate and damping rate of the oscillator.

We find the purity as

$$\mu = \frac{\gamma + \Gamma}{2\gamma\bar{n} + \gamma + \Gamma}. \tag{2.21}$$

For $\Gamma = 0$, This is $1/(2\bar{n}+1)$, the purity of a complectly mixed thermal state. For Γ very large, this tends to 1 and a highly pure state can be prepared. This equation clearly indicates that without thermal noise a highly pure state can be prepared. Fig. 2.2 shows that the purity is approaching to unity which indicates the possibility of creating a highly pure state.

2.4 Quadrature Squeezing of a Single Harmonic Oscillator

The question then arises whether or not it is possible to suppress the zero-point fluctuations of one quadrature via dissipation, this is known as squeezing. The engineered dissipative superoperator is something other than the oscillator lowering

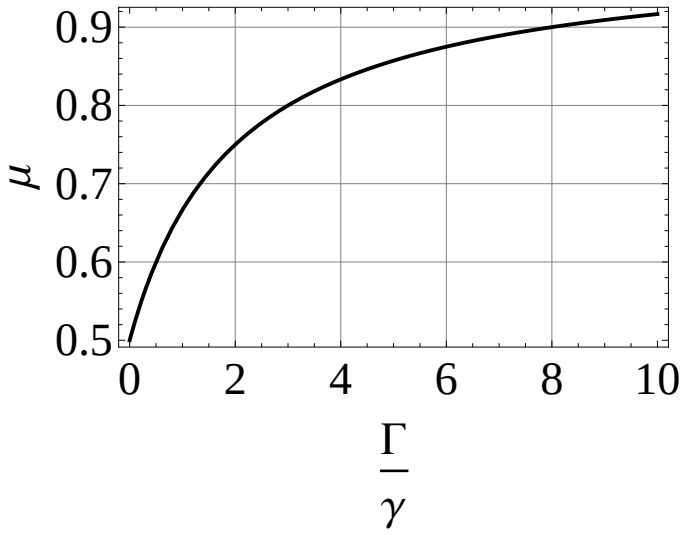

Figure 2.2: Purity of the steady-state of a single harmonic oscillator mode as a function of the ratio of coupling to a zero-temperature bath to coupling to a finite-temperature bath ($\bar{n} = 0.5$).

operator, the steady-state changes to (in the limit $\Gamma \gg \gamma$) the eigenstate corresponding to the zero eigenvalue of that operator. Indeed this is possible, and this has recently been demonstrated experimentally [38]. The master equation describing these dynamics is

$$\dot{\rho} = \gamma(\bar{n}+1)\mathcal{D}[\hat{a}]\rho + \gamma\bar{n}\mathcal{D}[\hat{a}^\dagger]\rho + \Gamma\mathcal{D}[\hat{\beta}]\rho. \tag{2.22}$$

If we choose $\hat{\beta}$ to be single-mode Bogoliubov operator as

$$\hat{\beta} = \hat{a}\cosh r + \hat{a}^\dagger \sinh r, \tag{2.23}$$

Then the eigenstate corresponding to the zero eigenvalue of this operator is none other than a squeezed state with squeezing parameter r [39]. The corresponding

dynamics for the second moments of system observables are

$$\frac{d}{dt}\begin{bmatrix}\langle\hat{a}^2\rangle\\ \langle\hat{a}^{\dagger 2}\rangle\\ \langle\hat{a}^\dagger\hat{a}\rangle\\ \langle\hat{a}\hat{a}^\dagger\rangle\end{bmatrix} = \begin{bmatrix}-\gamma-\Gamma & 0 & 0 & 0\\ 0 & -\gamma-\Gamma & 0 & 0\\ 0 & 0 & -\gamma-\Gamma & 0\\ 0 & 0 & 0 & -\gamma-\Gamma\end{bmatrix}\cdot\begin{bmatrix}\langle\hat{a}^2\rangle\\ \langle\hat{a}^{\dagger 2}\rangle\\ \langle\hat{a}^\dagger\hat{a}\rangle\\ \langle\hat{a}\hat{a}^\dagger\rangle\end{bmatrix} + \begin{bmatrix}-\Gamma\sinh r\cosh r\\ -\Gamma\sinh r\cosh r\\ \gamma\bar{n}+\Gamma\sinh r^2\\ \gamma+\gamma\bar{n}+\Gamma\cosh r^2\end{bmatrix}. \tag{2.24}$$

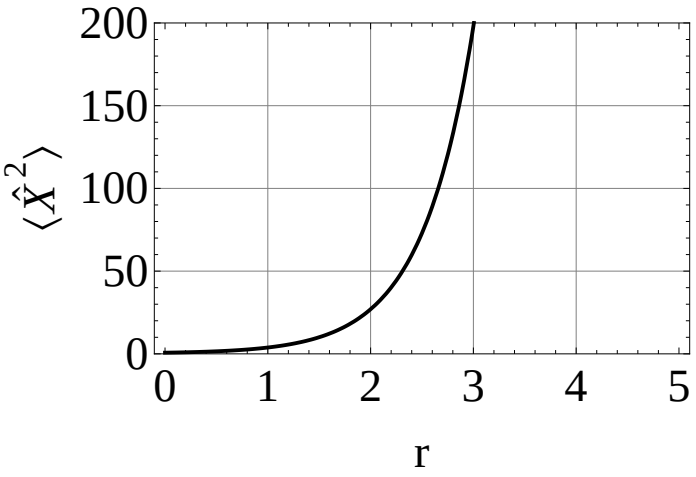

Figure 2.3: Second moment of the position quadrature $\langle\hat{X}^2\rangle$ against the squeezing parameter r.

Fig. 2.3 and 2.4 illustrate the gradual change of second moments of the quadrature operators $\hat{X}$ and $\hat{P}$ as a function of squeezing parameter r. The position quadrature operator variance $\langle\hat{X}^2\rangle$ increases exponentially with r (it is anti-squeezed), while the momentum quadrature operator variance $\langle\hat{P}^2\rangle$ decreases exponentially with r.

2.5 Collective Quadrature Squeezing of Two Harmonic Oscillator

Next we consider the possibility of dissipatively producing correlation between two oscillator modes. This will require non-local dissipative operators, which may be

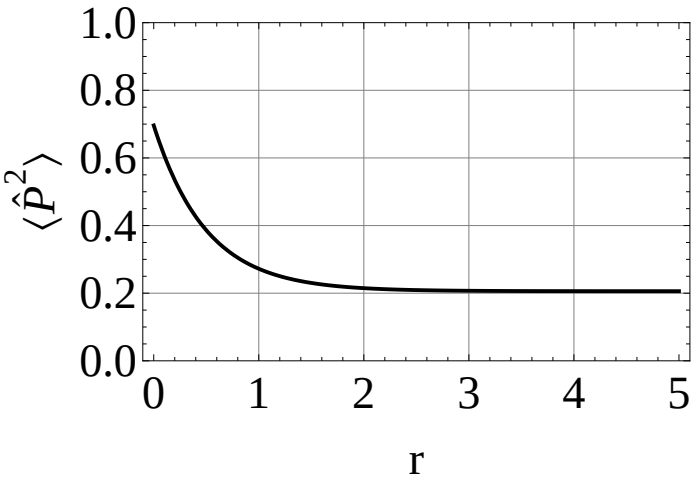

Figure 2.4: Second moment of the position quadrature $\langle \hat{P}^2 \rangle$ against the squeezing parameter r.

engineered via coupling to an auxiliary system. Let us consider the master equation as

$$\dot{\rho} = \Gamma_1 \mathcal{D}[\hat{\beta}_1]\rho + \Gamma_2 \mathcal{D}[\hat{\beta}_2]\rho + \gamma_a(\bar{n}_a+1)\mathcal{D}[\hat{a}]\rho + \gamma_b \bar{n}_b \mathcal{D}[\hat{a}^\dagger]\rho + \gamma_b(\bar{n}_b+1)\mathcal{D}[\hat{a}]\rho + \gamma_b \bar{n}_b \mathcal{D}[\hat{a}^\dagger]\rho, \tag{2.25}$$

where Γ_1 and Γ_2 are engineered damping rates, γ_a and γ_b are intrinsic damping rates, and $\bar{n}_a$ and $\bar{n}_b$ are thermal occupancy of the respective baths.

Now if we take $\hat{\beta}_1$ and $\hat{\beta}_2$ as two-mode Bogoliubov operators,

$$\hat{\beta}_1 = \hat{a}\cosh r + \hat{b}^\dagger \sinh r, \tag{2.26}$$

$$\hat{\beta}_2 = \hat{b}\cosh r + \hat{a}^\dagger \sinh r, \tag{2.27}$$

then the steady-state of the master equation in the limit $(\Gamma_1, \Gamma_2 \ll \gamma_a, \gamma_b)$ will be a (highly-entangled) two-mode squeezed state.

Fig. 2.5 and 2.6 show the change of $\langle \hat{X}_a^2 \rangle$ and $\langle \hat{P}_a^2 \rangle$ with respect to squeezing parameter r. The $\langle \hat{X}_a^2 \rangle$ and $\langle \hat{P}_a^2 \rangle$ is increased with the value of r; locally the oscillators are heated.

The simplest two-mode, continuous-variable entanglement criterion is the Duan

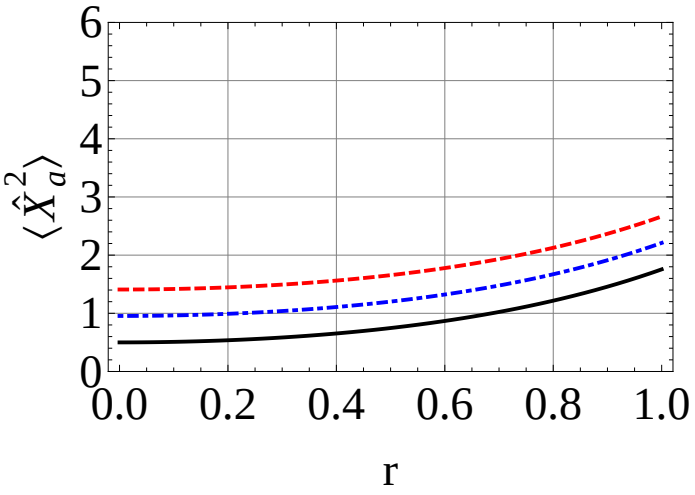

Figure 2.5: The change of second moment of position quadrature $\langle \hat{X}_a^2 \rangle$ with different thermal occupation baths as a function of squeezing parameter r. Here $\bar{n}_a = 0$, $\bar{n}_b = 0$ (black); $\bar{n}_a = 1$, $\bar{n}_b = 1$ (blue); and $\bar{n}_a = 5$, $\bar{n}_b = 0$ (red). Parameters taken for these curves are: $\gamma_{a,b} = 1$ and $\Gamma_{a,b} = 10$.

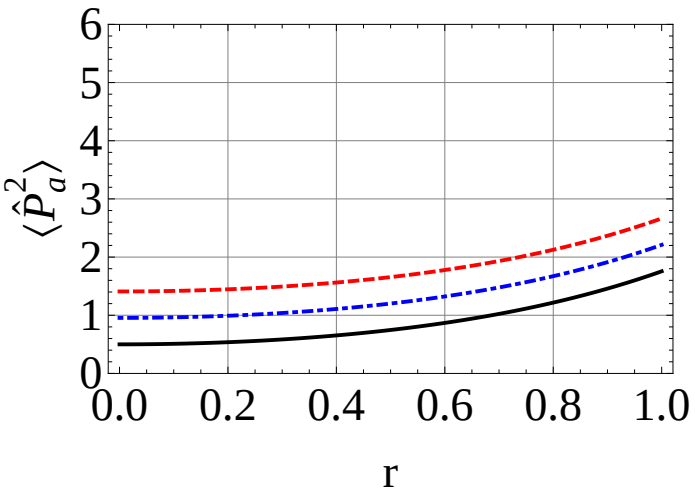

Figure 2.6: The change of second moment of momentum quadrature $\langle \hat{P}_a^2 \rangle$ with different thermal occupation baths as a function of squeezing parameter r. Here $\bar{n}_a = 0$, $\bar{n}_b = 0$ (black); $\bar{n}_a = 1$, $\bar{n}_b = 1$ (blue); and $\bar{n}_a = 5$, $\bar{n}_b = 0$ (red). Parameters taken for these curves are: $\gamma_{a,b} = 1$ and $\Gamma_{a,b} = 10$.

criterion. This is expressed in terms of collective quadratures operators defined by

$$\hat{X}_\pm = (\hat{X}_a \pm \hat{X}_b)/\sqrt{2}, \tag{2.28}$$

$$\hat{P}_\pm = (\hat{P}_a \pm \hat{P}_b)/\sqrt{2}, \tag{2.29}$$

where the usual quadratures for each oscillator mode are given by

$$\hat{X}_s = (\hat{s} + \hat{s}^\dagger)/\sqrt{2}, \tag{2.30}$$

$$\hat{P}_s = -i(\hat{s} + \hat{s}^\dagger)/\sqrt{2}. \tag{2.31}$$

The Duan criterion tells us that a Gaussian state for which [40]

$$\langle \hat{X}_+^2 \rangle + \langle \hat{P}_-^2 \rangle < 1, \tag{2.32}$$

is inseparable (that is, entangled). Note that this criterion could equally well be formulated in terms of $\langle \hat{X}_-^2 \rangle$ and $\langle \hat{P}_+^2 \rangle$. Fig. 2.7 illustrates that the Duan quantity is

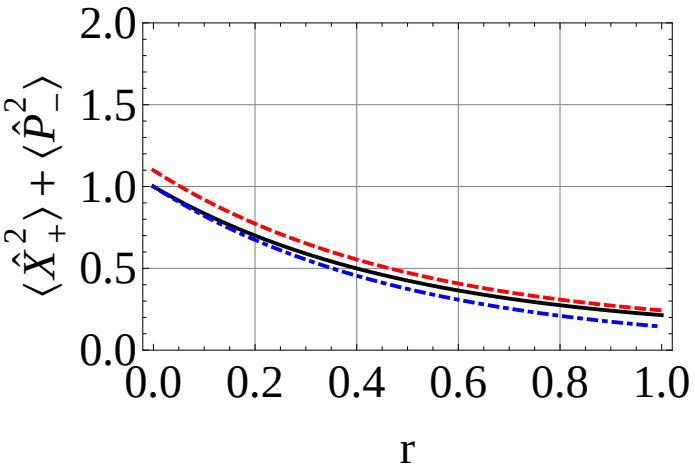

Figure 2.7: Duan quantity ($\langle \hat{X}_+^2 \rangle + \langle \hat{P}_-^2 \rangle$) plotted against squeezing parameter r with different thermal occupation baths. Here $\bar{n}_a = 0$, $\bar{n}_b = 0$ (black); $\bar{n}_a = 1$, $\bar{n}_b = 1$ (blue); and $\bar{n}_a = 5$, $\bar{n}_b = 0$ (red). Parameters taken for these curves are: $\gamma_{a,b} = 1$ and $\Gamma_{a,b} = 10$.

below one, which indicates that the oscillators are entangled in the steady state. In the cavity optomechanics context, beyond a fundamental state engineering demonstration, such states enable teleportation for quantum processing and force sensing beyond conventional quantum limits.

Chapter 3

Entanglement and Continuous-Variable Cluster States

In the preceding chapter we briefly described some Gaussian dissipative state engineering protocols. Such Gaussian states, assuming their first moments are zero, may be specified via their symmetrically-ordered covariance matrix in terms of oscillator quadrature operators. All of the interesting quantum noise properties of the state are encoded in the second moments. However, to go beyond one or two oscillator modes, it is useful to consider both how one can describe the correlations (including entanglement), and efficiently describe the states (leading us to the notion of cluster states).

3.1 Entanglement

A system consisting of a number of quantum subsystems is known as a composite quantum system. When those subsystems are entangled it is impossible to fully describe the state of one without making reference to the others. Entanglement is

most easily introduced starting with discrete variable systems. A simple example of a composite quantum system is a pair of two spin $-1/2$ particles in a singlet state

$$|\psi_{ab}\rangle = \frac{1}{\sqrt{2}}(|0\rangle_a|1\rangle_b + |1\rangle_a|0\rangle_b). \tag{3.1}$$

In this singlet states if a measurement of the z-component of the spin is made on one particle and found to be in the state $|0\rangle$, then the other will be found with certainty in the state $|1\rangle$. This property of entangled quantum states, has puzzled physicists all over the world. The paradoxical implications pointed out by Einstein, Podolsky and Rosen (EPR) in 1935 cast doubt on the acceptability of quantum mechanics as a consistent physical theory [41]. However, quantum mechanics has survived repeated empirical tests, most notably in experiments demonstrating the violation of Bell inequalities [42]. Singlet states described in Eq. (3.1) are now frequently called Bell states. Since entanglement represents non-local correlations that are independent of the observable to be measured, its characterization should be invariant under local transformations performed on the subsystems and be independent of the choice of the local basis.

If we consider a bipartite composite system in a pure state with wave function $|\psi_{ab}\rangle$, it is possible to find orthonormal bases $|i_a\rangle$ and $|i_b\rangle$ for systems a (of dimension N) and b (of dimension $M < N$) such that the joint state of the system can be written in the form

$$|\psi_{ab}\rangle = \sum_{i=1}^{N} \sqrt{p_i}|i_a\rangle \otimes |i_b\rangle, \tag{3.2}$$

where $p_i > 0$ and $\sum_{i=1}^{N} p_i = 1$. The so-called Schmidt coefficients p_i are uniquely defined for the state $|\psi_{ab}\rangle$ and are given by the eigenvalues of the reduced density matrix ρ_a and ρ_b as

$$\begin{aligned} \rho_a = \mathrm{Tr}_b \rho_{ab} = \mathrm{Tr}_b |\psi_{ab}\rangle\langle\psi_{ab}| &= \sum_{j=1}^{M} \langle J_b|\rho_{ab}|J_b\rangle \\ &= \sum_{i=1}^{N} p_i |i_a\rangle\langle i_a|. \end{aligned} \tag{3.3}$$

Hence they are automatically invariant under local unitary transformations.

The reduced density matrix [43] ρ_a is an essential description whenever a wave function cannot be attributed to a quantum subsystem A; i.e., when we do not have the maximal knowledge about the state allowed by quantum mechanics. It contains the correct statistics for measurements made on the system, since the expectation value of any observable A in the associated Hilbert space of the system can be determined by

$$\langle \hat{A} \rangle = \mathrm{Tr}(\hat{A}\rho_a). \tag{3.4}$$

Suppose a wave function ψ_a is associated with the subsystem with probability 1, i.e., $\mathrm{Tr}(\rho_a^2) = 1$, then the state is called a pure state. The density matrix is given by,

$$\rho_a = |\psi_a\rangle\langle\psi_a|. \tag{3.5}$$

For a pure state, we have the full knowledge about the state of the system allowed by quantum mechanics. Otherwise a system is in a mixed state, meaning we only have partial (or no) knowledge of the state allowed by quantum mechanics. Suppose the system is in one of state vectors $|\psi_1\rangle, |\psi_2\rangle, ...|\psi_N\rangle$ with probabilities p_i respectively. Then the density matrix for a mixed state can be written as

$$\rho_a = \sum_{i=1}^{N} p_i |\psi_i\rangle\langle\psi_i|, \tag{3.6}$$

where $\sum_{i=1}^{N} p_i = 1$.

From the above, one can see that for a pure state of the subsystem, the system is not entangled when considered as a whole. Therefore, the degree of impurity or classical uncertainty must be linked with the entanglement properties of the subsystems. An important measure of the bipartite (two-party) entanglement of a composite system in a pure state is the von Neumann entropy $S_N = \mathrm{Tr}(\rho_a \ln \rho_a)$. This measure will give zero for the separable state $|\psi_{ab}\rangle = |\psi_a\rangle|\psi_b\rangle$. They take the maximum value of unity for states in which the Schmidt coefficients are all equal

in magnitude. Unfortunately Schmidt decomposition does not apply for more than two entangled subsystems or for a bipartite system in mixed state.

3.1.1 Entanglement Measures

Entanglement description and quantification is an area of research in its own right. Much of the current work is motivated by the fact that entanglement is the key resource for both quantum communication and quantum computation. In the former, it enables non-classical protocols such as quantum teleportation [44] and superdense coding and leads to enhanced security in cryptographic tasks [45]. It is a key ingredient in determining the efficiency of quantum algorithms and quantum computation schemes [46]. In addition, entanglement raises new challenges and provides new resources in areas of quantum mechanics that are well established. Studies of entanglement have proved to be relevant to fields as different as atomic physics [47], quantum chaos [48–50], quantum phase transitions [51–53], and quantum networks [54].

As noted earlier for discrete-variable system, quantification of entanglement is a procedure closely related to a description revealing the different ways the parts can be entangled of a quantum system. There are some general requirements that an entanglement measure should satisfy. Aside from being invariant under local unitary transform actions, it should also decrease on average under general local operations [55]. The issue of quantification of entanglement in a mixed state is also of subject of research, even for bipartite systems. Prominent suggestions include the entanglement of formation and the distillable entanglement [56]; both difficult to compute except in the simplest of cases.

3.1.2 Logarithmic Negativity

An important class of entanglement measures are negativities, which quantify the violation of positive partial transposition (PPT) criterion for separability. We may write *Negativity* [57] as

$$N(\rho) = \frac{||\rho^{T_i}||_1 - 1}{2}, \tag{3.7}$$

where

$$||\hat{O}||_1 = Tr\sqrt{\hat{O}^\dagger \hat{O}}, \tag{3.8}$$

is the trace norm of the operator $\hat{O}$. The negativity is the computable measure of entanglement, being

$$N(\rho) = max\left\{0, -\sum_k \lambda_k^-\right\}, \tag{3.9}$$

where the $\{\lambda_k^-\}$ are the negative symplectic eignvalues of partial transpose. In continuous-variable systems, a related measure is more frequently used, this is called logarithmic negativity $E_n(\rho)$ [58, 59], which can be defined as

$$E_n(\rho) = log||\rho^{T_i}||_1 = log[1 + 2N(\rho)]. \tag{3.10}$$

3.2 Continuous-Variable Cluster State

Now we introduce continuous-variable cluster states, following the presentation of Ref. [60]. The basic CV cluster states are prepared with a collection of N zero-momentum eigenstates, which can be written as $|0\rangle_p^{\otimes N}$, where the p-subscripted kets satisfy $\hat{p}|s\rangle = s|s\rangle_p$. A collection of controlled-Z operations represented as $\hat{C}_z = e^{(ig\hat{q}\otimes\hat{q})}$, can be used to entangle these modes. Note that here, g is a real number which defines the strength of the interaction. As $\hat{C}_z$ operations commute, they can be applied to the modes in any order (or simultaneously).

Now we can construct a graphical representation for such cluster states. An example of such a graph is shown in Fig. 3.1. The zero-momentum eigenstates

are represented by nodes, and edges indicates a $\hat{C}_z$ operation to be performed between the two connected nodes. The strength g of the interaction is indicated by the label, or weight, of the associated edge. Such weighted graphs like this with real-valued weights can be used to map the ideal CV cluster states, which exhibit infinite squeezing (and are therefore unphysical). They are approximated by highly squeezed states.

The graph described can be compactly represented algebraically. Consider a symmetric adjacency matrix $\mathbf{A} = \mathbf{A}^T$ whose $(j,k)^{th}$ entry A_{jk} is equal to the weight of the edge linking node j to node k (with no edge corresponding to a weight of 0). Now the CV cluster state created with a collection of controlled-Z operations is a function of $\mathbf{A}$ which can be denoted by $\hat{C}_z[\mathbf{A}]$. The CV cluster state associated with graph $\mathbf{A}$ is then

$$\begin{aligned} |\psi_{\mathbf{A}}\rangle = \hat{C}_z[\mathbf{A}]|0\rangle_p^{\otimes N} &= \sum_{j,k=1}^{N} e^{\left(\frac{i}{2}\mathbf{A}_{jk}\hat{q}_j\hat{q}_k\right)}|0\rangle_p^{\otimes N} \\ &= exp\left(\frac{i}{2}\hat{\mathbf{q}}^T\mathbf{A}\hat{\mathbf{q}}\right)|0\rangle_p^{\otimes N} \end{aligned} \tag{3.11}$$

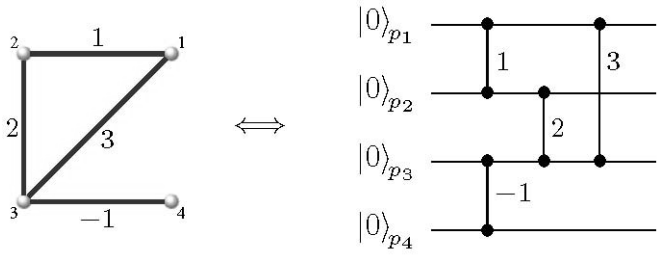

Figure 3.1: A CV cluster state represented as a weighted graph. Ideal (infinitely squeezed) CV cluster states are represented by undirected graphs with real-weighted edges. Unweighted graphs are a special case with all weights equal to 1. Each graph uniquely defines a recipe (i.e., a quantum circuit) for creating a CV cluster state, as illustrated: (1) each node represents a state that is infinitely squeezed in the $\hat{p}$ quadrature $|0\rangle_p$; and (2) C_z gates are applied between modes in accordance with the graph, with the weight g of an edge corresponding to the strength of the interaction $\hat{C}_z(g) = e^{ig\hat{q}\otimes\hat{q}}$ between the two nodes connected.

Note that here $\hat{\mathbf{q}} = (\hat{q}_1, ..., \hat{q}_n)^T$ is a column vector of Schrödinger picture

position operators. Due to the fact that each edge weight appears twice in the sum (as A_{jk} and as A_{kj}), the factor of 2 is essential. Ideal CV cluster states follow a set of so-called *nullifier* relations [61, 62], which can be written as

$$(\hat{\mathbf{p}} - \mathbf{A}\hat{\mathbf{q}})|\psi_{\mathbf{A}}\rangle = \mathbf{0}, \tag{3.12}$$

where $\hat{\mathbf{p}} = (\hat{p}_1, ..., \hat{p}_n)^T$ is a column vector of Schrödinger picture momentum operators. This equation actually represents N independent equations, one for each component of the vector $(\hat{\mathbf{p}} - \mathbf{A}\hat{\mathbf{q}})$, which are called *nullifiers* for the state $\psi_{\mathbf{A}}$ because that state is a simultaneous eigenstate corresponding to the zero eigenvalue.

A convenient graphical representation in terms of the adjacency matrix $\mathbf{A}$ is to be described for these ideal CV cluster states. We can quantify an approximate CV cluster indexed by an overall squeezing parameter α, for which

$$\lim_{\alpha\to\infty} cov(\hat{\mathbf{p}} - \mathbf{A}\hat{\mathbf{q}}) = \mathbf{0}, \tag{3.13}$$

where the covariance matrix of a vector of operators has components defined as the symmetrized expectation value

$$(cov\ \hat{\mathbf{r}})_{jk} = \frac{1}{2}\langle\{\hat{\mathbf{r}}_j^\dagger, \hat{\mathbf{r}}_k\}\rangle, \tag{3.14}$$

with $\hat{\mathbf{r}}$ denoting a vector of oscillator quadrature opearators. We may write the α-indexed approximate CV cluster state as $|\psi_{\mathbf{A}}(\alpha)\rangle$. Any α-indexed family of Gaussian pure states $\{|\psi_{\mathbf{A}}(\alpha)\rangle\}$ satisfying Eq. (3.14) represents a family of approximate CV cluster states described with graph $\mathbf{A}$. These Gaussian pure states can be used to describe a graphical formalism in a manner that takes into account their unique deviation from ideality.

However, a two-mode squeezed state is a Gaussian pure state but not approxi-

mate CV cluster state and it satisfies,

$$var(\hat{q}_1 - \hat{q}_2) = e^{-2\alpha}, \tag{3.15}$$

$$var(\hat{p}_1 + \hat{p}_2) = e^{-2\alpha}. \tag{3.16}$$

In the laboratory optical two-mode squeezed states are made by passage of position-squeezed and momentum-squeezed beams through a $50:50$ beamsplitter [63–65] or directly by nondegenerate parametric downconversion [63, 66–69]. These states do not satisfy Eq. (3.14) for any choice of (finitely weighted) graph $\mathbf{A}$, though they are α-indexed multimode squeezed state whose variances tend to 0 as $\alpha \to \infty$. That indicates they cannot be represented within the existing graphical formalism for CV cluster states [70]–even in the limiting case where $\alpha \to \infty$. This is unfortunate since the two-mode squeezed state is related to a two-mode CV cluster state by a Fourier transform on one of the modes–an LG unitary [62] that is one of the simplest to perform experimentally. That this equivalence cannot be represented in the graphical formalism–in either the ideal or the approximate case–is a significant drawback.

3.2.1 Matrix Formalism for Gaussian Pure States

We seek a matrix, and subsequently graphical, formalism capable of describing all pure Gaussian states. We want this matrix to be consistent with the formalism previously introduced for ideal CV cluster states. The complex-matrix formalism [71] for representing Gaussian pure states is now discussed. All N-mode Gaussian states can be created by acting on the ground state of N harmonic oscillators with a unitary operation whose Heisenberg action on the vector of quadrature operators is given by a symplectic transformation, followed by a phase-space displacement. These are sometimes called linear unitary Bogoliubov transformations [63]. We neglect the phase-space displacement altogether since we want the graphical formalism to describe the noise properties of the state, which do not depend on overall

displacement. Let us consider a column vector with $\hat{\mathbf{q}}$ on top of $\hat{\mathbf{p}}$ as

$$\hat{x} = \begin{bmatrix} \hat{\mathbf{q}} \\ \hat{\mathbf{p}} \end{bmatrix}. \tag{3.17}$$

The Heisenberg action of a Gaussian unitary operation $\hat{U}$ takes the form

$$\hat{\acute{\mathbf{x}}} = \hat{U}^{\dagger}\hat{\mathbf{x}}\hat{U} = \mathbf{S}\hat{\mathbf{x}}, \tag{3.18}$$

where $\mathbf{S}$ is a symplectic matrix of scalars that acts via matrix multiplication on $\hat{\mathbf{x}}$ as a vector, while $\hat{U}$ is a unitary operator that acts on the individual operators within $\hat{\mathbf{x}}$.

There is a unique $\mathbf{S}$ for every Gaussian $\hat{U}$, and there is a unique $\hat{U}$(up to an overall phase) for every symplectic $\mathbf{S}$. The symplectic nature of $\mathbf{S}$ is ensured because the commutation relations must be preserved, giving rise to a symplectic form $\mathbf{\Omega}$ to be preserved by the Heisenberg matrix action. The explicit form of $\mathbf{\Omega}$ can be obtained by the commutation relations for $\hat{x}$ and requiring them to be unchanged under the Gaussian unitary operation. The canonical commutation relations $[\hat{q}_j, \hat{p}_k] = i\delta_{jk}$ (with $\hbar = 1$) can be given by

$$[\hat{x}, \hat{x}^T] = i \begin{bmatrix} \mathbf{0} & \mathbf{I} \\ -\mathbf{I} & \mathbf{0} \end{bmatrix} = i\mathbf{\Omega}, \tag{3.19}$$

where the commutator of two operator-valued vectors is defined as

$$[\hat{\mathbf{r}}, \hat{s}^T] = \hat{\mathbf{r}}\hat{s}^T - (\hat{s}\hat{\mathbf{r}}^T)^T. \tag{3.20}$$

where the transpose operation acts only on the entries in the matrix (or vector), leaving the actual operators involved alone. The quadrature-operator commutators

remain unchanged after the Gaussian operation and this can be written as

$$i\mathbf{\Omega} = i\mathbf{S}\mathbf{\Omega}\mathbf{S}^T. \tag{3.21}$$

Now by canceling i's from both sides, this Eq. (3.21) is exactly the defining relation for any $2N \times 2N$ square matrix $\mathbf{S}$ to be a symplectic matrix with symplectic form $\mathbf{\Omega}$. This indicates the symplectic nature of $\mathbf{S}$ and required by the need to preserve the canonical commutation relations, which themselves play the role of the symplectic form $\mathbf{\Omega}$ (up to an overall factor of i), as shown in Eq. (3.19).

A covariance matrix can be used to describe a Gaussian pure state. We may express the symmetrized covariance matrix for an operator-valued vector as

$$cov\ \hat{\mathbf{r}} = \frac{1}{2}\langle\{\hat{\mathbf{r}}^\dagger, \hat{\mathbf{r}}^T\}\rangle, \tag{3.22}$$

which accords with Eq. (3.14). If we define the anti-commutator product as

$$\{\hat{\mathbf{r}}, \hat{s}^T\} = \hat{\mathbf{r}}\hat{s}^T + (\hat{s}\hat{\mathbf{r}}^T)^T. \tag{3.23}$$

Since every N-mode Gaussian pure state can be obtained by acting with a Gaussian unitary operation on the ground state of N independent harmonic oscillators, we can use the symplectic representation of this operation to parameterise these states. By eliminating units in $\hat{\mathbf{q}}$ and $\hat{\mathbf{p}}$, the covariance matrix of the N-mode ground state can be written as

$$cov\ \hat{x}_0 = \frac{1}{2}\mathbf{I}, \tag{3.24}$$

where $\hat{x}_0$ is the vector of Heisenberg operators associated with this state. This indicates that $var\ \hat{q}_{0j} = var\ \hat{p}_{0j} = \frac{1}{2}$ for every mode j, where var and cov stands for variance and covariance respectively. The Heisenberg operators for any Gaussian pure state can be obtained from x_0 by acting with a symplectic matrix. The

resulting covariance matrix can be written in terms of a symplectic matrix as

$$cov\ \hat{\mathbf{x}} = \frac{1}{2}\mathbf{S}\mathbf{S}^T. \tag{3.25}$$

Since the covariance matrix uniquely defines a Gaussian state, so does $\mathbf{S}\mathbf{S}^T$. Now we have to create a graph representation of $\mathbf{S}\mathbf{S}^T$ to be practically useful for our purposes. Therefore, we will decompose $\mathbf{S}$ and use the resulting matrix factors to define the adjacency matrix for an associated graph. There are a number of ways to decompose a symplectic matrix, but the one we are interested in is the following particular decomposition for any symplectic $\mathbf{S}$ [71]:

$$\mathbf{S} = \begin{bmatrix} \mathbf{I} & \mathbf{0} \\ \mathbf{V} & \mathbf{I} \end{bmatrix} \begin{bmatrix} \mathbf{U}^{-1/2} & \mathbf{0} \\ \mathbf{0} & \mathbf{U}^{-1/2} \end{bmatrix} \begin{bmatrix} \mathbf{X} & -\mathbf{Y} \\ \mathbf{Y} & \mathbf{X} \end{bmatrix}, \tag{3.26}$$

where $\mathbf{U}$ is symmetric and positive definite ($\mathbf{U} = \mathbf{U}^T > 0$), $\mathbf{V}$ is symmetric (but not necessarily positive definite), and the third matrix is orthogonal and thus irrelevant in the product $\mathbf{S}\mathbf{S}^T$. This expansion is unique for a given $\mathbf{S}$, and since we only care about $\mathbf{S}\mathbf{S}^T$, we can define $\mathbf{X} = \mathbf{I}$ and $\mathbf{Y} = \mathbf{0}$ and, after multiplying the right-hand side above, we have

$$\mathbf{S}_{(\mathbf{U},\mathbf{V})} = \begin{bmatrix} \mathbf{U}^{-1/2} & \mathbf{0} \\ \mathbf{V}\mathbf{U}^{-1/2} & \mathbf{U}^{-1/2} \end{bmatrix}. \tag{3.27}$$

Using Eq. (3.25), the covariance matrix associated with this state is

$$V_{(\mathbf{U},\mathbf{V})} = \frac{1}{2}\mathbf{S}_{(\mathbf{U},\mathbf{V})}\mathbf{S}^T_{(\mathbf{U},\mathbf{V})} = \frac{1}{2}\begin{bmatrix} \mathbf{U}^{-1} & \mathbf{U}^{-1}\mathbf{V} \\ \mathbf{V}\mathbf{U}^{-1} & \mathbf{U} + \mathbf{V}\mathbf{U}^{-1}\mathbf{V} \end{bmatrix}. \tag{3.28}$$

This is a very useful expression of covariance matrix of a pure Gaussian state through graphical formalism. Since the state is pure, the position space wave func-

tion can be given as

$$\psi_{(\mathbf{U},\mathbf{V})}(\mathbf{q}) = \pi^{-N/4}(det\ \mathbf{U})^{1/4} exp\ [\frac{1}{2}\mathbf{q}^T(\mathbf{U} - i\mathbf{V})\mathbf{q}]. \tag{3.29}$$

Note that $\mathbf{q}, \mathbf{p}$, and $\mathbf{x} = \begin{bmatrix} \mathbf{q} \\ \mathbf{p} \end{bmatrix}$ are scalar column vectors that correspond to their respective operator-valued counterparts. Eqs. (3.27), (3.28) and (3.29) can be used to define a Gaussian pure state from any pair of $N \times N$ symmetric matrices, $\mathbf{U}$ and $\mathbf{V}$, with $\mathbf{U} > 0$ ensuring the physicality of the state. Eq. (3.27) defines the Heisenberg quadrature variables $\hat{\mathbf{x}} = \mathbf{S}_{(\mathbf{U},\mathbf{V})}\hat{\mathbf{x}}_0$ associated with the state in question, where Eq. (3.28) gives the (symmetrized) covariance matrix, and Eq. (3.29) gives the wave function of the state. Inversion of these relations to find $\mathbf{U}$ and $\mathbf{V}$ is straightforward. The ground state corresponds to $\mathbf{U} = \mathbf{I}$ and $\mathbf{V} = \mathbf{0}$.

The complex combination $\mathbf{U} - i\mathbf{V}$ that appears in Eq. (3.29) is suggestive of a way to unify the two symmetric matrices that define a Gaussian pure state. After multiplication by i, we get

$$\mathbf{Z} = \mathbf{V} + i\mathbf{U}. \tag{3.30}$$

We define $\mathbf{Z}$ as the adjacency matrix for an undirected graph with complex-valued edge weights, thus providing our graph representation for any Gaussian pure state.

3.3 Approximate CV Cluster State

The graph representative of a Gaussian pure state discussed above is, in fact, the most effective way to extend the graph representation of ideal CV cluster state to their finitely squeezed Gaussian approximations. The canonical method for obtaining a CV cluster state [72] is to squeeze all modes as much as possible in the momentum quadrature and then to apply $\hat{C}_Z[\mathbf{A}]$ in accord with a (real-weighted) graph $\mathbf{A}$. An ideal cluster state $|\psi_{\mathbf{A}}\rangle$ from Eq. (3.11) is obtained by taking the limit of infinite initial squeezing on all the modes. Now let us consider this scenario in

the graphical formalism [73, 74].

The symplectic transformation corresponding to the canonically generated CV cluster state consists of two parts: the initial single-mode squeezing and the controlled-Z operations. If we take all modes to be momentum squeezed with their variance reduced by a factor of e^{-2r}, followed by the controlled $\hat{C}_Z[\mathbf{A}]$ operations, this corresponds to a total symplectic transformation of

$$\begin{bmatrix} \mathbf{I} & \mathbf{0} \\ \mathbf{A} & \mathbf{I} \end{bmatrix} \begin{bmatrix} e^r\mathbf{I} & \mathbf{0} \\ \mathbf{0} & e^r\mathbf{I} \end{bmatrix}. \tag{3.31}$$

Comparing this with Eq. (3.27), we can immediately read off that $\mathbf{U} = e^{2r}\mathbf{I}$ and $\mathbf{V} = \mathbf{A}$, and we find that

$$\mathbf{Z}_r = \mathbf{A} + ie^{-2r}\mathbf{I}, \tag{3.32}$$

corresponds to an r-indexed family of approximate CV cluster states with graph $\mathbf{A}$ since

$$\lim_{r\to\infty} \mathbf{Z}_r = \mathbf{A}. \tag{3.33}$$

3.4 Complex Nullifiers

We can generalize the real-valued nullifier formalism to complex-valued nullifiers, which can be used to represent Gaussian pure states. The nullifier formalism for CV cluster states, given by Eq. (3.12), can be extended to all Gaussian pure states using the simple replacement of the CV cluster-state graph $\mathbf{A}$ with the Gaussian graph $\mathbf{Z}$:

$$\begin{aligned} (\hat{\mathbf{p}} - \mathbf{Z}\hat{\mathbf{q}})|\psi_{\mathbf{z}}\rangle &= (-\mathbf{Z}\ \mathbf{I})\hat{\mathbf{x}}\hat{\mathbf{U}}_{\mathbf{z}}|0\rangle \\ &= \hat{U}_{\mathbf{z}}(-\mathbf{Z}\ \mathbf{I})\mathbf{S}_{\mathbf{z}}\hat{\mathbf{x}}|0\rangle \\ &= \hat{U}_{\mathbf{z}}\mathbf{U}^{1/2}(\hat{\mathbf{p}} - i\hat{\mathbf{q}})|0\rangle \\ &= \mathbf{0}, \end{aligned} \tag{3.34}$$

where we have used Eq. (3.27) to substitute for $S_{\mathbf{z}} = \mathbf{S}_{(\mathbf{U},\mathbf{V})}$, and we note that $\hat{\mathbf{p}} - i\hat{\mathbf{q}} = -i\sqrt{2}\hat{\mathbf{a}}$, is a vector of operators annihilating the ground state. Here the *nullifier vector* $\hat{\mathbf{p}} - \mathbf{Z}\hat{\mathbf{q}}$ is not unique for a given graph since any matrix of scalar $\mathbf{M}$ acting from the left, will generate a new vector of nullifiers for the state. In the case of the ground state, $\mathbf{Z} = i\mathbf{I}$. we can calculate

$$cov\ [\hat{\mathbf{p}} - \mathbf{Z}\hat{\mathbf{q}}] = \mathbf{U}. \tag{3.35}$$

For approximate CV cluster states, it is also necessary to calculate the covariance matrix of just the real part of $\mathbf{Z}$ (namely, $\mathbf{V}$):

$$cov\ [\hat{\mathbf{p}} - \mathbf{V}\hat{\mathbf{q}}] = \frac{1}{2}\mathbf{U}. \tag{3.36}$$

Comparing this expression with Eq. (3.33), we end up with a nice interpretation of $\mathbf{Z}$'s real and imaginary parts: $\mathbf{V}$ is the graph of the ideal CV cluster state approximated by $\mathbf{Z}$, and $\frac{1}{2}\mathbf{U}$ is the error in the approximation. For this interpretation to make any sense, $\mathbf{U}$ must be small. If $\mathbf{U} > 0$, we can use the trace to say that $\frac{1}{2}tr\mathbf{U}$ is the magnitude of the approximation error in approximating the ideal CV cluster state $\mathbf{V}$ using $\mathbf{Z}$.

In summary, we have presented the generalisation of the real nullifier formalism for real-weighted ideal CV cluster states to a complex nullifier formalism for complex-weighted, physical CV cluster states, as well as all other Gaussian pure states.

Chapter 4

Preparation of Entangled States in Multimode Optomechanics

4.1 System and Hamiltonian

Techniques for the preparation of entangled states of two mechanical modes, two optical modes, or one mechanical and one optical mode, have previously been described. Here we consider the preparation of tripartite entangled states. Consider a system composed of three mechanical oscillators coupled to three electromagnetic cavity modes. The electromagnetic cavity mode may take the form of an optical cavity [37] or a microwave circuit [75]; the underlying physics is very similar. For the sake of concreteness, here we focus on the microwave circuit case [30]. Hence, the development of the Hamiltonian will be framed in terms of the capacitance of an electrical circuit rather than the radiation pressure of an optical field. Suppose the cavity modes have resonance frequencies $\omega_{c,k}$ for cavity $k = 1, 2, 3$ and the mechanical oscillators have resonance frequencies $\omega_{m,j}$ and mass m_j for oscillator $j = 1, 2, 3$. The uncoupled electromagnetic cavities may be described by a lumped-element equivalent inductance L_k and equivalent capacitance C_k. Assuming that the amplitude of the mechanical oscillators motion is small compared with

the equilibrium separation between the oscillators and the microwave circuit. The capacitive coupling to linear-order, between cavity k and mechanical oscillator j is

$$C_{jk}(x_j) = C_{0,jk}\left(1 - x_j/d_{jk}\right), \tag{4.1}$$

where x_j is the position of the mechanical oscillator, d_{jk} is the equilibrium separation between the mechanical oscillator and microwave cavity, and $C_{0,jk}$ is the equilibrium capacitance. The effective capacitance of each cavity is $C_{\Sigma,k} = C_k + \sum_{j=1}^{3} C_{0,jk}$, such that the coupled resonance frequency is $\omega_{c,k} = 1/\sqrt{L_k C_{\Sigma,k}}$. Consequently, the system is described by the classical Hamiltonian

$$H = \sum_{j=1}^{3}\left(\frac{p_j^2}{2m_j} + \frac{1}{2}m_j\omega_{m,j}^2 x_j^2\right) + \sum_{k=1}^{3}\left(\frac{\Phi_k^2}{2L_k} + \frac{Q_k^2}{2C_{\Sigma,k}}\right) + \sum_{j,k=1}^{3}\frac{\beta_{jk}}{2d_{jk}C_{\Sigma,k}}x_j Q_k^2 + \sum_{j=1}^{3}\sum_{k=1}^{3}\frac{1}{2}[e_{+jk}(t) + e_{-jk}(t)]Q_k, \tag{4.2}$$

where p_j is the momentum of mechanical oscillator j, Φ_k is the flux through the inductance and Q_k is the change on the capacitance of microwave circuit k. The coupling between the mechanical oscillator and microwave circuits are given by $\beta_{jk} = C_{jk}/C_{\Sigma,k}$, and the cavities are driven at frequencies $\omega_{d,\pm jk}$, according to the electric potential

$$e_{\pm jk}(t) = 2\sqrt{2\hbar\omega_c L}(\varepsilon_{\pm jk}e^{+i\omega_{d,\pm jk}t} + \text{c.c.}), \tag{4.3}$$

with $\varepsilon_{\pm jk}$ denote driving fields as the microwave circuit mode k.

We may quantize the Hamiltonian by imposing the commutation relations $[\hat{x}_m, \hat{p}_n] = i\hbar\delta_{mn}$ and $[\hat{Q}_m, \hat{\Phi}_n] = i\hbar\delta_{mn}$. In the Schrödinger picture, we have

$$\hat{H}_s = \sum_{j=1}^{3}\hbar\omega_{m,j}\hat{b}_j^\dagger\hat{b}_j + \sum_{k=1}^{3}\hbar\omega_{c,k}\hat{a}_k^\dagger\hat{a}_k + \sum_{j,k=1}^{3}\frac{1}{2}\hbar\kappa_{jk}(\hat{b}_j + \hat{b}_j^\dagger)(\hat{a}_k + \hat{a}_k^\dagger)^2 + \sum_{j=1}^{3}\sum_{k=1}^{3}\hbar(\hat{a}_k + \hat{a}_k^\dagger)(\varepsilon_{+jk}e^{+i\omega_{d,+jk}t} + \varepsilon_{-jk}e^{+i\omega_{d,-jk}t} + \text{c.c.}). \tag{4.4}$$

where the circuit and mechanical oscillator lowering operators are

$$\hat{a}_k = \sqrt{\frac{\omega_{c,k} L_k}{2\hbar}} \hat{Q}_k + \frac{i}{\sqrt{2\hbar\omega_{c,k} L_k}} \hat{\Phi}_k, \tag{4.5}$$

$$\hat{b}_j = \sqrt{\frac{m_j \omega_{m,j}}{2\hbar}} \hat{x}_j + \frac{i}{\sqrt{2\hbar m_j \omega_{m,j}}} \hat{p}_j, \tag{4.6}$$

respectively and the coupling constants are

$$\kappa_{jk} = \frac{\beta_{jk} \omega_{c,k} \Delta x_j}{2 d_{jk}}, \tag{4.7}$$

with $\Delta x_j = \sqrt{\hbar / 2 m_j \omega_{m,j}}$ being the width of the quantum ground state for mechanical oscillator j.

Suppose the cavities are driven on *one sideband* ($\varepsilon_{-jk} = 0$) and by moving into an interaction picture making a rotating-wave approximation with respect to

$$\hat{H}_0^1 = \sum_{k=1}^{3} \hbar\omega_{d,jk} \hat{a}_k^\dagger \hat{a}_k + \sum_{j=1}^{3} \hbar\omega_{m,j} \hat{b}_j^\dagger \hat{b}_j, \tag{4.8}$$

we find

$$\hat{H}_I^1 = \sum_{j,k=1}^{3} \hbar\delta_{+jk} \hat{a}_k^\dagger \hat{a}_k + \sum_{j,k=1}^{3} \hbar\kappa_{jk} (\hat{b}_j e^{-i\omega_{m,j} t} + \hat{b}^\dagger e^{+i\omega_{m,j} t}) \hat{a}_k^\dagger \hat{a}_k + \sum_{j=1}^{3} \sum_{k=1}^{3} \hbar(\varepsilon_{+jk} \hat{a}_k + \text{H.c.}), \tag{4.9}$$

where $\delta_{+jk} = \omega_{c,k} - \omega_{d,+jk}$ are the detuning parameters. Here $\delta_{\pm jk} > 0$ denotes driving on blue sideband and $\delta_{\pm jk} < 0$ denotes driving on red sideband. Alternatively, we may consider driving the circuits on both red and the blue sidebands. To do so we move into an interaction picture with respect to the Hamiltonian

$$\hat{H}_0^2 = \sum_{j=1}^{3} \hbar\omega_{m,j} \hat{b}_j^\dagger \hat{b}_j + \sum_{k=1}^{3} \hbar\omega_{c,k} \hat{a}_k^\dagger \hat{a}_k, \tag{4.10}$$

leaves

$$\hat{H}_I^2 = \sum_{j,k=1}^{3} \hbar\kappa_{jk}(\hat{b}_j e^{-i\omega_{m,j}t} + \hat{b}^\dagger e^{+i\omega_{m,j}t})\hat{a}_k^\dagger \hat{a}_k + \sum_{j=1}^{3}\sum_{k=1}^{3} \hbar(\varepsilon_{+jk}\hat{a}e^{+i\delta_{+jk}t} + \varepsilon_{-jk}\hat{a}e^{+i\delta_{-jk}t} + \text{H.c.}). \tag{4.11}$$

The terms with κ_{jk} represent a low-frequency modulation, at the mechanical resonance frequency, of the cavity resonance frequency. Note that this coupling has the same form as the dispersive radiation pressure coupling well-known in cavity optomechanics. This interaction also writes sidebands onto the cavity transmission spectrum at integer multiples of the mechanical resonance frequencies. By driving the cavities on these sidebands, the cavity fields on resonance couple to the slowly-varying quadratures of the mechanical oscillator motion.

4.2 Quantum Langevin Equation

The internal losses of microwave circuits can be small compared with the damping due to out-coupling of the field, such that the circuits may function as good transducers. Further, it is assumed that the mechanical oscillators undergo a quantum Brownian motion [76]. This assumption, combined with the fact that we may subsequently linearise the optomechanical interaction, means that we shall use a quantum Langevin equation approach rather than a master equation approach. Now the Hamiltonian described in Eq. (4.11) and the assumption of linear damping and a Gaussian white noise [77] input fields leads to the quantum Langevin equation as

$$\dot{\hat{a}}_k = -i\sum_{j=1}^{3} \kappa_{jk}(\hat{b}_j e^{-i\omega_{m,j}t} + \hat{b}^\dagger e^{+i\omega_{m,j}t})\hat{a}_k - i\sum_{j=1}^{3}(\varepsilon_{+jk}e^{-i\delta_{+jk}t} + \varepsilon_{-jk}e^{-i\delta_{-jk}t}) - \frac{\mu_k}{2}\hat{a}_k + \sqrt{\mu_k}\hat{a}_{k,in}, \tag{4.12}$$

$$\dot{\hat{b}}_j = -i\sum_{k=1}^{3} \kappa_{jk}e^{i\omega_{m,j}t}\hat{a}_k^\dagger \hat{a}_k - \frac{\gamma_j}{2}\hat{b}_j + \sqrt{\gamma_j}\hat{b}_{j,in}. \tag{4.13}$$

The associated non-zero input noise correlation functions are

$$\langle \hat{a}_{k,in}(t), \hat{a}^{\dagger}_{k,in}(t') \rangle = \delta(t - t'), \tag{4.14}$$

$$\langle \hat{b}^{\dagger}_{j,in}(t), \hat{b}_{j,in}(t') \rangle = \bar{n}_{m,j}\delta(t - t'), \tag{4.15}$$

where $\bar{n}_{m,j}$ is the thermal occupancy of the mechanical bath at the mechanical resonance frequency, and the correlations used is defined by

$$\langle \hat{A}, \hat{B} \rangle = \langle \hat{A}\hat{B} \rangle - \langle \hat{A} \rangle \langle \hat{B} \rangle. \tag{4.16}$$

The thermal occupancy is given by the Bose-Einstein distribution (phonons are bosons) by

$$\bar{n}_{m,j} = \left[exp\left(\frac{\hbar\omega_{m,j}}{k_B T_{m,j}} \right) - 1 \right]^{-1}. \tag{4.17}$$

where k_B is the Boltzmann constant, and $T_{m,j}$ is the effective mechanical bath temperature. It is assumed that the microwave circuit is at a sufficiently high frequency that it may be assumed to be damped into a zero-temperature bath.

4.3 Effective Hamiltonian

As the cavity quality factors are assumed to be very large (i.e., we are in the so-called resolved sideband regime, also known as the good cavity limit), we can decompose the microwave fields into sideband modes as,

$$\hat{a}_k(t) = \sum_{j=1}^{3} [\hat{a}_{+jk}(t)e^{-i\omega_{m,j}t} + \hat{a}_{-jk}(t)e^{+i\omega_{m,j}t}] + \hat{a}_{0k}(t), \tag{4.18}$$

$$\hat{b}_j(t) = \hat{b}_j(t), \tag{4.19}$$

where $'-'$ refers to the blue sideband components and $'+'$ refers to the red sideband components. Let us assume the cavity driving right on the mechanical sidebands i.e., $\delta_{\pm jk} = \pm\omega_{m,j}$. Substituting these into Eqs. (4.12) and (4.13) and equating

frequency components, we obtain

$$\dot{\hat{a}}_{0k}(t) = -i\sum_{j=1}^{3}\kappa_{jk}[\hat{b}_j(t)\hat{a}_{-jk}(t) + \hat{b}_j^{\dagger}(t)\hat{a}_{+jk}(t)] - \frac{\mu_{0k}}{2}\hat{a}_{0k}(t) + \sqrt{\mu_{0k}}\hat{a}_{0k,in}(t), \tag{4.20}$$

$$\dot{\hat{a}}_{\pm jk}(t) = -i\kappa_{\pm jk}[\hat{b}_j(t)\hat{a}_{0k}(t)] - i\varepsilon_{\pm jk} - \frac{\mu_{\pm jk}}{2}\hat{a}_{\pm jk}(t) + \sqrt{\mu_{\pm jk}}\hat{a}_{\pm jk,in}(t), \tag{4.21}$$

and

$$\dot{\hat{b}}_j = -i\sum_{k=1}^{3}\kappa_{jk}[\hat{a}_{0k}^{\dagger}(t)\hat{a}_{+jk}(t) + \hat{a}_{-jk}^{\dagger}(t)\hat{a}_{0k}(t)] - \frac{\gamma_j}{2}\hat{b}_j(t) + \sqrt{\gamma_j}\hat{b}_{j,in}(t). \tag{4.22}$$

Initially neglecting the effect of the weak bare optomechanical coupling, we have the steady-state amplitudes as

$$\langle\hat{a}_{\pm jk}\rangle_{ss} = \pm\frac{i\varepsilon_{\pm jk}}{(i\omega_{m,j} - \mu_{\pm jk})}, \tag{4.23}$$

where $\mu_{\pm jk}$ are the cavity damping rates as a function of cavity index k and mechanical oscillator index j. Now using these values and dropping the sideband subscripts of Eqs. (4.20) and (4.21), we obtain the reduced system of quantum Langevin equations,

$$\dot{\hat{a}}_k(t) = -i\sum_{j=1}^{3}[g_{-jk}\hat{b}_j(t) + g_{+jk}\hat{b}_j^{\dagger}(t)] - \frac{\mu_k}{2}\hat{a}_k(t) + \sqrt{\mu_k}\hat{a}_{k,in}(t), \tag{4.24}$$

$$\dot{\hat{b}}_j(t) = -i\sum_{k=1}^{3}[g_{+jk}\hat{a}_k^{\dagger}(t) + g_{-jk}\hat{a}_k(t)] - \frac{\gamma_j}{2}\hat{b}_j(t) + \sqrt{\gamma_j}\hat{b}_{j,in}(t), \tag{4.25}$$

where, $g_{\pm jk}$ are the effective couplings in this optomechanical system

$$g_{\pm jk} = \pm\kappa_{jk}\frac{i\varepsilon_{\pm jk}}{(i\omega_{m,j} - \mu_{\pm jk})}. \tag{4.26}$$

As three mechanical resonators coupled with three cavities via two driving tones, there exists 18 different coupling parameters on which the dynamics of our system

depend.

By using Eq. (4.24) and Eq. (4.25), we may obtain the effective Hamiltonian of our multimode optomechanical system as

$$\hat{H}_{\text{eff}} = \hbar \sum_{j,k=1}^{3} [g_{+jk} a_k b_j + g_{-jk} a_k^\dagger b_j + \text{H.c.}]. \tag{4.27}$$

4.4 Adiabatic Elimination of Cavity Modes

Assuming damping of the mechanical oscillators into thermal baths with occupations $\bar{n}_{m,j}$, the quantum optics master equation describing our system dynamics may be written as

$$\dot{\rho} = -\frac{i}{\hbar}[\hat{H}_{\text{eff}}, \rho] + \sum_{j=1}^{3} \gamma_j (\bar{n}_{m,j} + 1)\mathcal{D}[\hat{b}_j]\rho + \sum_{j=1}^{3} \gamma_j \bar{n}_{m,j} \mathcal{D}[\hat{b}_j^\dagger]\rho + \sum_{k=1}^{3} \mu_k \mathcal{D}[\hat{a}_k]\rho. \tag{4.28}$$

where $\hat{H}_{\text{eff}}$ is the Hamiltonian given in Eq. (4.27). Now we assume that the circuit modes are heavily damped such that cavity mode at the sideband of the driving field will have few photons and will be slaved to the mechanical oscillator modes. This is the appropriate limit for the circuits to be good transducers of the mechanical oscillators motion. More precisely, this regime corresponds to our parameters being chosen such that [78]

$$| \frac{g_{\pm jk}}{\mu_k} | \ll 1. \tag{4.29}$$

Then the cavity modes may be adiabatically eliminated from the description of the system. This procedure yields the master equation for the three mechanical oscillators modes,

$$\dot{\rho}_{\text{m}} = \sum_{j=1}^{3} \gamma_j (\bar{n}_{m,j} + 1)\mathcal{D}[\hat{b}_j]\rho_{\text{m}} + \sum_{j=1}^{3} \gamma_j \bar{n}_{m,j} \mathcal{D}[\hat{b}_j^\dagger]\rho_{\text{m}} + \sum_{k=1}^{3} \Gamma_k \mathcal{D}[\hat{N}_k]\rho_{\text{m}}, \tag{4.30}$$

where the Hamiltonian dynamics of Eq. (4.27) has been incorporated into a modified dissipative dynamics in Eq. (4.28). The new effective damping rates are $\Gamma_k =$

$4g_k^2/\mu_k$, with $g_k = \max_j \{g_{\pm jk}/\bar{g}_{\pm jk}\}$. The forms of the operators $\hat{N}_k$ depend on the cavity driving conditions, and we can set the $\hat{N}_k$ to be an arbitrary linear combination of mechanical quadrature operators by choosing $g_{\pm jk}$ (i.e., the driving conditions) appropriately. If we set the driving conditions such that $\hat{N}_k$ correspond to the nullifiers of a three-mode continuous variable cluster state [60], then in the limit $\Gamma_k \gg \gamma_j(\bar{n}_{mj} + 1)$, such a tripartite-entangled mechanical cluster state can be prepared with high fidelity.

4.5 Tripartite Mechanical Steady States

Recall that in a graphical representation of the CV cluster state each vertex of the graph corresponds to a mode, and the edges corresponds to the application of an entangling operation between the connected modes. A canonical CV cluster state can be specified by r-indexed matrix $\mathbf{Z}_r$ in the Eq. (3.32) at Section 2.5. To find this $\mathbf{Z}_r$ we have to calculate the adjacency matrix $\mathbf{A}$ for undirected graph with real-valued edge weights. We can assume adjacency matrix $\mathbf{A}$ by using schematic diagram of our system in linear and triangular structure as shown in Fig. 4.1.

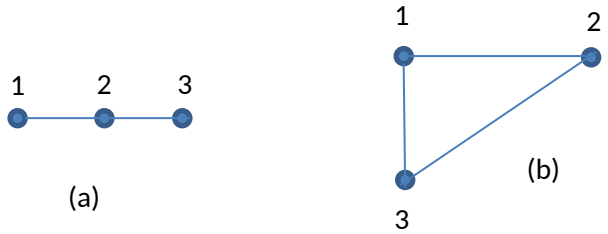

Figure 4.1: Two different tripartite cluster states, where 1, 2, and 3 denote the three target modes of the reduced system description. (a) Schematic diagram of linear structure. (b) Schematic diagram of triangular structure.

For a linear tripartite cluster state we assume the real-valued adjacency matrix from Fig. 4.1(a) as

$$\mathbf{A}_L = \begin{bmatrix} 0 & 1 & 0 \\ 1 & 0 & 1 \\ 0 & 1 & 0 \end{bmatrix}, \tag{4.31}$$

and for triangular structure from the Fig. 4.1(b) we have

$$\mathbf{A}_T = \begin{bmatrix} 0 & 1 & 1 \\ 1 & 0 & 1 \\ 1 & 1 & 0 \end{bmatrix}. \tag{4.32}$$

The adjacency matrix with complex-valued edge weights for both structures calculated are simply

$$\mathbf{Z}_L = \begin{bmatrix} ie^{-2r} & 1 & 0 \\ 1 & ie^{-2r} & 1 \\ 0 & 1 & ie^{-2r} \end{bmatrix}, \tag{4.33}$$

$$\mathbf{Z}_T = \begin{bmatrix} ie^{-2r} & 1 & 1 \\ 1 & ie^{-2r} & 1 \\ 1 & 1 & ie^{-2r} \end{bmatrix}. \tag{4.34}$$

By using Eq. (4.33) the nullifiers for the linear structure are found as to be,

$$\hat{N}_1 = \left(-\frac{i}{\sqrt{2}} - \frac{ie^{-2r}}{\sqrt{2}}\right)\hat{b}_1 + \left(\frac{i}{\sqrt{2}} - \frac{ie^{-2r}}{\sqrt{2}}\right)\hat{b}_1^\dagger - \frac{\hat{b}_2}{\sqrt{2}} - \frac{\hat{b}_2^\dagger}{\sqrt{2}} \tag{4.35}$$

$$\hat{N}_2 = \left(\frac{i}{\sqrt{2}} - \frac{ie^{-2r}}{\sqrt{2}}\right)\hat{b}_2 + \left(-\frac{i}{\sqrt{2}} - \frac{ie^{-2r}}{\sqrt{2}}\right)\hat{b}_2^\dagger - \frac{\hat{b}_1}{\sqrt{2}} - \frac{\hat{b}_1^\dagger}{\sqrt{2}} - \frac{\hat{b}_3}{\sqrt{2}} - \frac{\hat{b}_3^\dagger}{\sqrt{2}}, \tag{4.36}$$

$$\hat{N}_3 = \left(-\frac{i}{\sqrt{2}} - \frac{ie^{-2r}}{\sqrt{2}}\right)\hat{b}_3 + \left(\frac{i}{\sqrt{2}} - \frac{ie^{-2r}}{\sqrt{2}}\right)\hat{b}_3^\dagger - \frac{\hat{b}_1}{\sqrt{2}} - \frac{\hat{b}_1^\dagger}{\sqrt{2}}. \tag{4.37}$$

where $\hat{b}_j$ denote the lowering operators for the mechanical oscillator modes. Similarly for the triangular structure we find the nullifiers to be

$$\hat{N}_1 = \left(-\frac{i}{\sqrt{2}} - \frac{ie^{-2r}}{\sqrt{2}}\right)\hat{b}_1 + \left(\frac{i}{\sqrt{2}} - \frac{ie^{-2r}}{\sqrt{2}}\right)\hat{b}_1^\dagger - \frac{\hat{b}_2}{\sqrt{2}} - \frac{\hat{b}_2^\dagger}{\sqrt{2}} - \frac{\hat{b}_3}{\sqrt{2}} - \frac{\hat{b}_3^\dagger}{\sqrt{2}}, \tag{4.38}$$

$$\hat{N}_2 = \left(\frac{i}{\sqrt{2}} - \frac{ie^{-2r}}{\sqrt{2}}\right)\hat{b}_2 + \left(-\frac{i}{\sqrt{2}} - \frac{ie^{-2r}}{\sqrt{2}}\right)\hat{b}_2^\dagger - \frac{\hat{b}_1}{\sqrt{2}} - \frac{\hat{b}_1^\dagger}{\sqrt{2}} - \frac{\hat{b}_3}{\sqrt{2}} - \frac{\hat{b}_3^\dagger}{\sqrt{2}}, \tag{4.39}$$

$$\hat{N}_3 = \left(\frac{i}{\sqrt{2}} - \frac{ie^{-2r}}{\sqrt{2}}\right)\hat{b}_3 + \left(-\frac{i}{\sqrt{2}} - \frac{ie^{-2r}}{\sqrt{2}}\right)\hat{b}_3^\dagger - \frac{\hat{b}_1}{\sqrt{2}} - \frac{\hat{b}_1^\dagger}{\sqrt{2}} - \frac{\hat{b}_2}{\sqrt{2}} - \frac{\hat{b}_2^\dagger}{\sqrt{2}}. \tag{4.40}$$

.

We have seen that the required nullifiers for a given tripartite entangled steady state are associated with the cavity driving conditions of our multimode optomechanical system. We can get the required couplings comparing the $\hat{N}_k$ with Eq. (4.28) and Eq. (4.30). The required coupling rate for the linear tripartite entangled state nullifiers $\hat{N}_1$ are

$$\bar{g}_{+11} = \frac{1}{\sqrt{2}}(i - ie^{-2r}), \bar{g}_{-11} = -\frac{1}{\sqrt{2}}(i + ie^{-2r}), \bar{g}_{+21} = -\frac{1}{\sqrt{2}},$$
$$\bar{g}_{-21} = -\frac{1}{\sqrt{2}}, \bar{g}_{+31} = 0, \bar{g}_{-31} = 0. \tag{4.41}$$

For the nullifiers $\hat{N}_2$ we require

$$\bar{g}_{+12} = -\frac{1}{\sqrt{2}}, \bar{g}_{-12} = -\frac{1}{\sqrt{2}}, \bar{g}_{+22} = \frac{1}{\sqrt{2}}(i - ie^{-2r}),$$
$$\bar{g}_{-22} = -\frac{1}{\sqrt{2}}(i + ie^{-2r}), \bar{g}_{+32} = -\frac{1}{\sqrt{2}}, \bar{g}_{-32} = -\frac{1}{\sqrt{2}}, \tag{4.42}$$

and for the nullifiers $\hat{N}_3$ we require the coupling rates

$$\bar{g}_{+13} = -\frac{1}{\sqrt{2}}, \bar{g}_{-13} = -\frac{1}{\sqrt{2}}, \bar{g}_{+23} = 0,$$
$$\bar{g}_{-23} = 0, \bar{g}_{+33} = \frac{1}{\sqrt{2}}(i - ie^{-2r}), \bar{g}_{-33} = -\frac{1}{\sqrt{2}}(i + ie^{-2r}). \tag{4.43}$$

Similarly, we can also calculate the effective coupling rates in case of triangular tripartite cluster state. For the nullifiers $\hat{N}_1$ we require the effective couplings

$$\bar{g}_{+11} = \frac{1}{\sqrt{2}}(i - ie^{-2r}), \bar{g}_{-11} = -\frac{1}{\sqrt{2}}(i + ie^{-2r}), \bar{g}_{+22} = -\frac{1}{\sqrt{2}},$$
$$\bar{g}_{-22} = -\frac{1}{\sqrt{2}}, \bar{g}_{+33} = -\frac{1}{\sqrt{2}}, \bar{g}_{-33} = -\frac{1}{\sqrt{2}}. \tag{4.44}$$

For $\hat{N}_2$ we require the effective couplings,

$$\bar{g}_{12} = -\frac{1}{\sqrt{2}}, \bar{g}_{-13} = -\frac{1}{\sqrt{2}}, \bar{g}_{+22} = \frac{1}{\sqrt{2}}(i - ie^{-2r}),$$

$$\bar{g}_{-22} = -\frac{1}{\sqrt{2}}(i + ie^{-2r}), \bar{g}_{+32} = -\frac{1}{\sqrt{2}}, \bar{g}_{-32} = -\frac{1}{\sqrt{2}}, \tag{4.45}$$

and for $\hat{N}_3$ we require the effective couplings

$$\begin{aligned} \bar{g}_{+13} = -\frac{1}{\sqrt{2}}, \bar{g}_{-13} = -\frac{1}{\sqrt{2}}, \bar{g}_{+23} = -\frac{1}{\sqrt{2}}, \\ \bar{g}_{-23} = -\frac{1}{\sqrt{2}}, \bar{g}_{+33} = \frac{1}{\sqrt{2}}(i - ie^{-2r}), \bar{g}_{-33} = -\frac{1}{\sqrt{2}}(i + ie^{-2r}). \end{aligned} \tag{4.46}$$

The complete specification of the effective coupling rates tells us the amplitude and phases of the microwave circuit driving tones required for the generation of a tripartite entangled mechanical steady-state.

4.6 Experimentally Feasible Parameter

In this section we will discuss the experimentally accessible parameters for our system. The microwave circuit resonance frequencies will be $\omega_{c,k} = 2\pi \times \{5.8, 6, 6.2\}$ GHz [79] and the mechanical oscillators resonance frequencies will be $\omega_{m,j} = 2\pi \times 18, 20, 22$ MHz [80]. The cavity impedance should be $50\,\Omega$, with an equivalent inductance $L = 1.33\,\text{nH}$ and an equivalent capacitance $C = 0.531\,\text{pF}$. Assuming a mechanical oscillator of mass $10^{-15}\,\text{kg}$, the ground state uncertainty in the mechanical oscillator position is $\Delta x = 20.5\,\text{fm}$. We may also assume an equilibrium mechanical oscillators to microwave circuit separation of $d_{jk} = 80\,\text{nm}$ and $\beta_{jk} = 0.002$, then $\kappa_{jk} = 9.6\,\text{s}^{-1}$. Microwave cavities can be fabricated with quality factor $Q_k = 10^5$ and mechanical oscillators with quality factor $Q_m = 10^5$, the corresponding damping rates are around $\mu_k = 3.77 \times 10^5\,\text{s}^{-1}$ and $\gamma_j = 1.26 \times 10^3\,\text{s}^{-1}$. The effective fiducial coupling $g/\mu_k = 0.09$ corresponds to $\varepsilon = 4.441 \times 10^{11}\,\text{s}^{-1}$, and a photon number at the drive frequency of $n_c = 1.249 \times 10^7$. This corresponds to the effective (engineered) damping rates around $\Gamma = 5.49 \times 10^5\,\text{s}^{-1}$. The key point is that these engineered mechanical damping rate greatly exceed the intrinsic damping rates of the mechanical oscillators. Hence, one would expect that the tripartite mechanical

cluster states may be prepared with high fidelity.

Chapter 5

Characterisation of Entanglement in Multimode Optomechanics

Given a master equation description of the dynamics of the multimode cavity optomechanics system in terms of an effective Hamiltonian, we have determined the parameter and driving conditions required for the preparation of a given entangled tripartite steady state. Now to characterise the entanglement in this system we need to determine the steady-state covariance matrix. One approach is to write down a linear system for the second moments of all modes using the master equation. However, since the effective system is linear, the steady-state covariance matrix may be obtained in a straightforward manner from the linear quantum Langevin equation.

5.1 Linear Quantum System Approach

Recall that a dissipative system with n degrees of freedom associated with the density matrix $\rho(t)$ is governed by the Markovian master equation as [81, 82]

$$\dot{\rho} = -\frac{i}{\hbar}[\hat{H}, \hat{\rho}] + \sum_{k=1}^{m} \Gamma_k \mathcal{D}[\hat{L}_k]\rho, \tag{5.1}$$

where $\hat{L}_k$ is the the k^{th} dissipative channel that represents the coupling between the system and environmental degree of freedom. For a linear quantum system, Hamiltonian $\hat{H}$ and dissipative operators (sometimes called cryogenic operators) $\hat{L}_k$ may be written as

$$\begin{aligned} \hat{H} =& \frac{1}{2}\hat{x}^T G \hat{x}, \\ \hat{L}_k =& C_k^T \hat{x}, \end{aligned} \tag{5.2}$$

where G is a real-valued, symmetric Hamiltonian matrix with $G = G^T \epsilon \mathbf{R}^{2n\times 2n}$, and C_k is a complex valued vector with $G = C_k \epsilon \mathbf{C}^{2n}$. Now $\hat{x} := (\hat{q}_1, ..., \hat{q}_n, \hat{p}_1, ..., \hat{p}_n)^T$ is a vector of quadrature operators, which satisfy the commutation relations

$$\hat{x}\hat{x}^T - (\hat{x}\hat{x}^T)^T = i\Sigma, \Sigma = \begin{bmatrix} 0 & I_n \\ -I_n & 0 \end{bmatrix}. \tag{5.3}$$

As for a system of (classical) linear stochastic differential equations, the evolution of the system's symmetrically-ordered covariance matrix V is given by a time dependent Lyapunov equation [83]

$$\frac{dV}{dt} = AV + VA^T + D, \tag{5.4}$$

with the drift matrix

$$A = \Sigma[G + \mathrm{Im}(C^\dagger C)], \tag{5.5}$$

and the diffusion matrix

$$D = \Sigma \mathrm{Re}(C^\dagger C)\Sigma^T. \tag{5.6}$$

where $C = (c_1, ..., c_m)^T \epsilon \mathbf{C}^{m\times 2n}$. If the system is in a steady state, then a covariance

matrix V_s will be a unique solution to this following matrix Lyapunov equation:

$$AV_s + V_s A^T + D = 0. \tag{5.7}$$

Then the steady state covariance matrix is readily calculated. From the steady-state covariance matrix we are well-placed to study the entanglement properties of the steady-state.

Figs. 5.1 and 5.2 show the gradual decrease of purity with the increase of squeezing parameter r

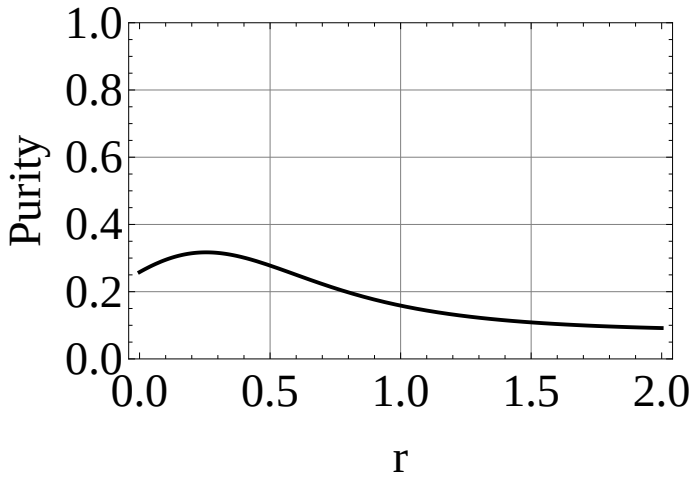

Figure 5.1: Purity of tripartite cluster states (linear) with dissipation against squeezing parameter r.

5.2 Bipartite Entanglement

A complete qualitative characterisation of the bipartite entanglement of a three-mode Gaussian state is possible because the positivity of partial transpose (PPT) criterion is necessary and sufficient for their separability under any, partial or global, bipartition. This has led to an exhaustive classification of three-mode Gaussian states into five distinct classes [84]. These classes take into account the fact that the modes 1, 2, and 3 allow for three distinct bipartitions, where i, j, and k represent

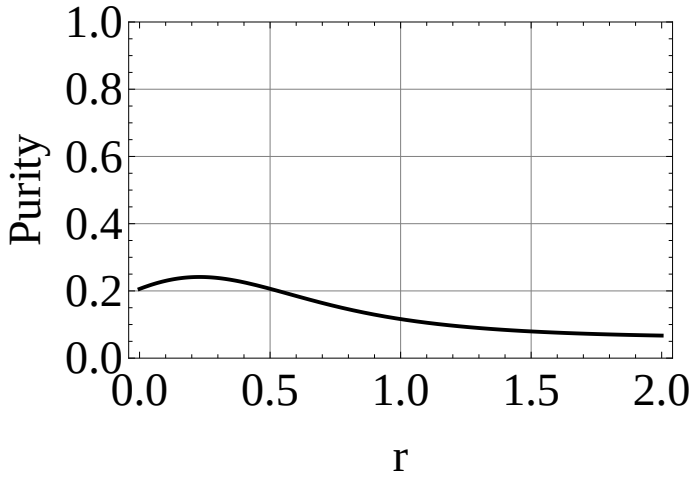

Figure 5.2: Purity of tripartite cluster states (triangular) with dissipation against squeezing parameter r.

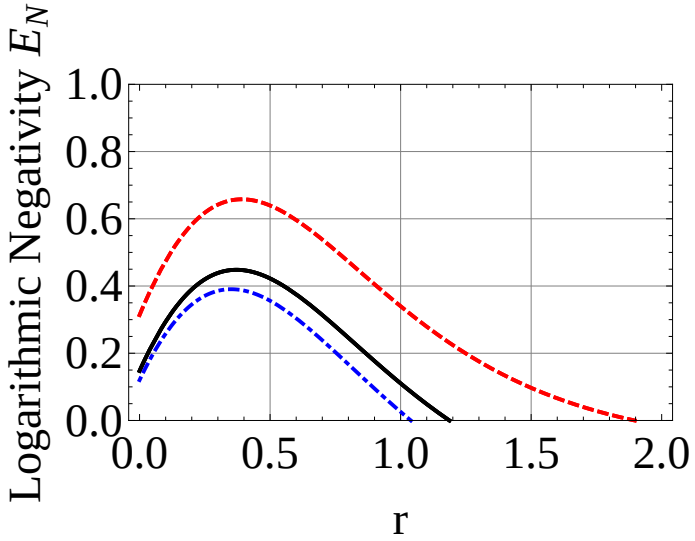

Figure 5.3: Bipartite entanglement, (quantified by logarithmic Negativity) against squeezing parameter r for a triangular (solid line) and linear (dashed line) tripartite cluster state. Note that all bipartitions of the triangular cluster state have the same entanglement, while this is not the case of the linear cluster state.

all possible permutations:

✓Class 1: states not separable under all three possible bipartitions $i \times (jk)$ of the modes (fully inseparable states, possessing genuine multipartite entanglement).

✓Class 2: states separable under only one of the three possible bipartitions (one mode biseparable states).

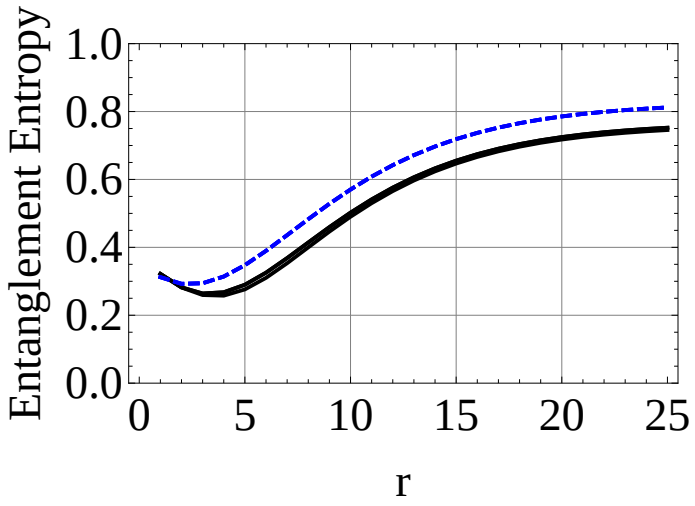

Figure 5.4: Bipartite entanglement, (quantified by logarithmic Negativity) against squeezing parameter r for a triangular (solid line) and linear (dashed line) tripartite cluster state.

✓Class 3: states separable under only two of the three possible bipartitions (two mode biseparable states).

✓Class 4: states separable under all the three possible bipartitions, but impossible to write as a convex sum of the tripartite products of pure one-mode states (three-mode biseparable states).

✓Class 5: states that are separable under all three possible bipartitions, and can be written as a convex sum of tripartite products of pure one mode states (fully separable states).

Note that classes 4 and 5 cannot be distinguished by partial transposition of any of the three modes (which is positive for both classes). States in class 4 stand therefore as nontrivial examples of tripartite entangled states with positive partial transpose.

There are different measures of entanglement for bipartite states. In our study we consider all possible reduced two-mode bipartitions for both the linear and triangular cluster state structures. The bipartite entanglement is studied using logarithmic negativity. Now from Eq. (3.10), we may write the logarithmic negativity

as [85]

$$E_n = \max\{0, -\ln 2\chi\}, \tag{5.8}$$

where,

$$\chi = 2^{-1/2}\{\Sigma(V) - [\Sigma(V)^2 - 4\mathrm{Det}V]^{1/2}\}^{1/2}, \tag{5.9}$$

with

$$\Sigma(V) = \mathrm{Det}V_b + \mathrm{Det}V_a - 2\mathrm{Det}V_{ab}. \tag{5.10}$$

where V_a and V_b denote the covariance matrix of subsystem a and b, respectively, and V_{ab} is the covariance matrix between subsystems a and b.

We have calculated an r-indexed covariance matrix from approximate CV cluster state with graph **A** for both linear and triangular cluster state structures. The logarithmic negativity for linear structure have same value for $E_{n(12)}$ and $E_{n(23)}$ and as expected different for $E_{n(13)}$. These results are given below–

$$E_{n(12)} = -\ln\left[\sqrt{2}\sqrt{\frac{1}{2} + \frac{5e^{4r}}{4} - \sqrt{-\frac{1}{16} + \left(\frac{1}{2} + \frac{5e^{4r}}{4}\right)^2}}\right], \tag{5.11}$$

$$E_{n(23)} = -\ln\left[\sqrt{2}\sqrt{\frac{1}{2} + \frac{e^{4r}}{2} - \sqrt{-\frac{1}{16} + \left(\frac{1}{2} + \frac{e^{4r}}{2}\right)^2}}\right], \tag{5.12}$$

$$E_{n(13)} = -\ln\left[\sqrt{2}\sqrt{\frac{1}{2} + \frac{5e^{4r}}{4} - \sqrt{-\frac{1}{16} + \left(\frac{1}{2} + \frac{5e^{4r}}{4}\right)^2}}\right]. \tag{5.13}$$

For the triangular structure the logarithmic negativity is found to be the same between all bipartitions.

$$E_{n(12)} = E_{n(23)} = E_{n(13)} = -\ln\left[\sqrt{2}\sqrt{\frac{1}{2} + \frac{3e^{4r}}{2} - \sqrt{-\frac{1}{16} + \left(\frac{1}{2} + \frac{3e^{4r}}{2}\right)^2}}\right], \tag{5.14}$$

as is to be expected given the symmetry present in the cluster state structures.

All reduced two mode bipartitions for both cases are plotted in the Fig 5.5 with

respect to the squeezing parameter r. Here all the logarithmic negativity measured for bipartite states are greater than zero, which indicates the existence of bipartite entanglement between all subsystems.

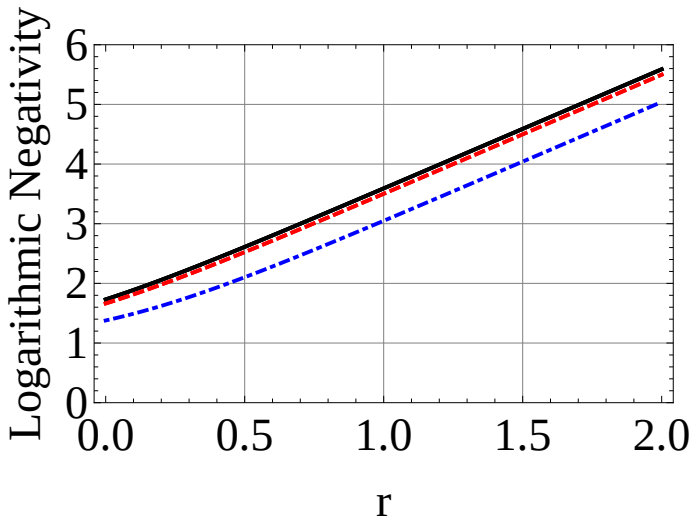

Figure 5.5: The Bipartite entanglement, quantified by the logarithmic negativity against squeezing parameter r for a triangular (solid line) and linear (dashed line) tripartite cluster state. Note that all bipartitions give the same entanglement for the triangular structure, but there are two different values for the linear structure due to the symmetry of the state.

These results may be compared with these of Fig. 5.3 describing the logarithmic negativity accounting for additional dissipative mechanisms.

5.3 Tripartite Entanglement

We can also characterize genuine tripartite entanglement via the Gaussian Rényi-2 entanglement entropy [86]. Let us recall that the form of any Gaussian state can be simplified through (unitary) symplectic operations. Up to local unitaries, the standard form of covariance matrix $V_{A_iA_jA_k}$ of any pure three-mode continuous-

variable cluster state is written as

$$V_{A_iA_jA_k} = \begin{bmatrix} a_1 & 0 & e_{12}^{+} & 0 & e_{13}^{+} & 0 \\ 0 & a_2 & 0 & e_{12}^{-} & 0 & e_{13}^{-} \\ e_{12}^{+} & 0 & a_2 & 0 & e_{23}^{+} & 0 \\ 0 & e_{12}^{-} & 0 & a_2 & 0 & e_{23}^{-} \\ e_{13}^{+} & 0 & e_{23}^{+} & 0 & a_3 & 0 \\ 0 & e_{13}^{-} & 0 & e_{23}^{-} & 0 & a_3 \end{bmatrix}, \tag{5.15}$$

with

$$\begin{aligned} e_{ij}^{\pm} = & \frac{\sqrt{[(a_i - a_j)^2 - (a_k - 1)^2][(a_i - a_j)^2 - (a_k + 1)^2]}}{4\sqrt{a_i a_j}} \\ & \pm \frac{\sqrt{[(a_i + a_j)^2 - (a_k - 1)^2][(a_i + a_j)^2 - (a_k + 1)^2]}}{4\sqrt{a_i a_j}}, \end{aligned} \tag{5.16}$$

here a_i is related to the covariance matrix V_i of subsystem i:

$$a_i = \sqrt{\mathrm{Det} V_i}. \tag{5.17}$$

The Rényi-2 entropy is defined as

$$S_2(\rho) = -\ln \mathrm{Tr}(\rho^2). \tag{5.18}$$

The tripartite entanglement can be characterize by the systems bipartite states as

$$\varepsilon_2(\rho_{A_i:A_j:A_k}) = \varepsilon_2(\rho_{A_i:A_jA_k}) - \varepsilon_2(\rho_{A_i:A_j}) - \varepsilon_2(\rho_{A_i:A_k}), \tag{5.19}$$

where $\varepsilon_2(\rho_{A_i:A_jA_k})$ is the bipartite entanglement partitioning the global system into A_i and A_jA_K, $\varepsilon_2(\rho_{A_i:A_j})$ and $\varepsilon_2(\rho_{A_i:A_k})$ is the entanglement entropy of subsystem A_iA_j and A_iA_K. Now three different values of $\varepsilon_2(\rho_{A_i:A_j:A_k})$ are possible, depending on the choice of the three modes A_i, A_j and A_k. For pure tripartite Gaussian state, the entanglement entropy $\varepsilon_2(\rho_{A_i:A_jA_k})$ is given by,

$$\varepsilon_2(\rho_{A_i:A_jA_k}) = S_2(\rho_i) = \ln a_i. \tag{5.20}$$

Also the entanglement entropy for two-mode reduced states $\varepsilon_2(\rho_{A_i:A_j})$ and $\varepsilon_2(\rho_{A_i:A_k})$ can be given as,

$$\varepsilon_2(\rho_{A_i:A_j}) = \frac{1}{2}\ln\ g_k, \tag{5.21}$$

$$\varepsilon_2(\rho_{A_i:A_k}) = \frac{1}{2}\ln\ g_j, \tag{5.22}$$

where

$$g_k = \begin{cases} 1, & \text{if } a_k \geq \sqrt{a_i^2 + a_j^2 - 1} \\ \frac{\beta}{8a_k^2}, & \text{if } \alpha_k < a_k < \sqrt{a_i^2 + a_j^2 - 1} \\ \left(\frac{a_i^2 - a_j^2}{a_k - 1}\right)^2, & \text{if } a_k \leq \alpha_k \end{cases} \tag{5.23}$$

and

$$g_j = \begin{cases} 1, & \text{if } a_j \geq \sqrt{a_i^2 + a_k^2 - 1} \\ \frac{\beta}{8a_j^2}, & \text{if } \alpha_j < a_j < \sqrt{a_i^2 + a_k^2 - 1} \\ \left(\frac{a_i^2 - a_k^2}{a_j - 1}\right)^2, & \text{if } a_j \leq \alpha_j \end{cases}, \tag{5.24}$$

with

$$\alpha_k = \sqrt{\frac{2(a_i^2 + a_j^2) + (a_i^2 - a_j^2) + |a_i^2 - a_j^2|\sqrt{(a_i^2 - a_j^2)^2 + 8(a_i^2 + a_j^2)}}{2(a_i^2 + a_j^2)}}, \tag{5.25a}$$

$$\alpha_j = \sqrt{\frac{2(a_i^2 + a_k^2) + (a_i^2 - a_k^2) + |a_i^2 - a_k^2|\sqrt{(a_i^2 - a_k^2)^2 + 8(a_i^2 + a_k^2)}}{2(a_i^2 + a_k^2)}}, \tag{5.25b}$$

$$\beta = -1 + 2a_1^2 + 2a_3^2 + 2a_3^2 + 2a_1^2a_2^2 + 2a_1^2a_3^2 + 2a_2^2a_2^3 - a_1^4 - a_2^4 - a_3^4 - \sqrt{\delta}, \tag{5.25c}$$

$$\delta = (-1 + a_1 - a_2 - a_3)(1 + a_1 - a_2 - a_3)(-1 + a_1 + a_2 - a_3)(1 + a_1 + a_2 - a_3) \tag{5.25d}$$

$$\times(-1+a_1-a_2+a_3)(1+a_1-a_2+a_3)(-1+a_1+a_2+a_3)(1+a_1+a_2+a_3). \tag{5.25e}$$

Now using Eqs. (5.23) and (5.25a), we can calculate the residual Gaussian Rényi-2 (GR2) entanglement entropy, with respect to the focus mode A_i as

$$\varepsilon_2(\rho_{A_i:A_j:A_k}) = \frac{1}{2}\ln\left(\frac{a_i^2}{g_k g_j}\right). \tag{5.26}$$

By using the same method, the residual Gaussian Rényi-2 entanglement entropy can be calculated, with respect to focus mode A_j and A_k as

$$\varepsilon_2(\rho_{A_j:A_i:A_k}) = \frac{1}{2}\ln\left(\frac{a_j^2}{g_k g_i}\right), \tag{5.27}$$

$$\varepsilon_2(\rho_{A_k:A_i:A_j}) = \frac{1}{2}\ln\left(\frac{a_k^2}{g_i g_j}\right). \tag{5.28}$$

Now by using the covariance matrix for our system, mapped from r-indexed approximate continuous-variable cluster state, we have calculated $\varepsilon_2(\rho_{A_i:A_j:A_k})$, $\varepsilon_2(\rho_{A_j:A_i:A_k})$ and $\varepsilon_2(\rho_{A_k:A_i:A_j})$ for both linear and triangular tripartite cluster state structures. The results are plotted in Fig. 5.6. We consider all the relevant cases of a fully inseparable three-mode pure Gaussian states and all the residual GR2 entanglement entropy are nonzero, which confirms the presence of genuine tripartite entanglement.

These results of GR2 entanglement entropy may be compared with these of Fig. 5.4 accounting for additional dissipative mechanisms.

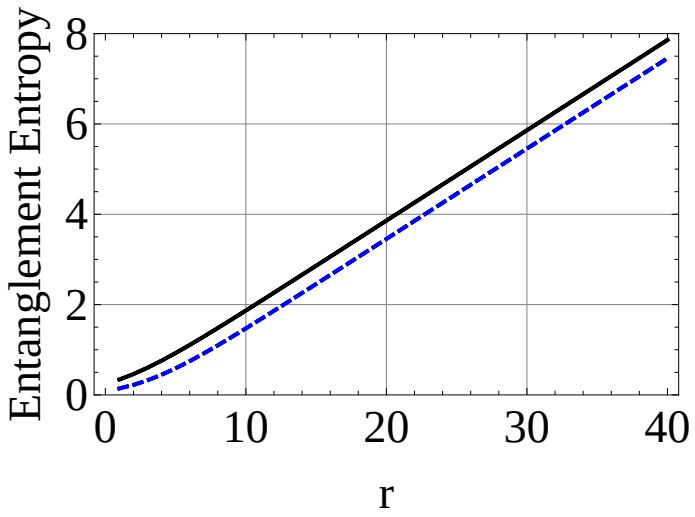

Figure 5.6: Genuine tripartite mechanical entanglement, (quantified by the residual GR2 entanglement) against squeezing parameter r for a triangular (solid line) and linear (dashed line) tripartite cluster state.

Chapter 6

Conclusion and Future Research

6.1 Conclusion

This thesis has discussed the preparation and characterisation of tripartite entangled states of mechanical oscillators in a multimode cavity optomechanical system. The model consists of three electromagnetic cavities coupled with three micromechanical oscillators.

The basic theory of quantum optomechanics, and the physics necessary for our investigation was introduced in chapter 1. This began with a treatment of the basic harmonic oscillator, followed by a quantum mechanical view of electromagnetic and mechanical oscillators, introduction to cavity optomechanics, and a general Markovian master equation formulation was briefly discussed. The optomechanical coupling and determination of optomechanical equations of motion from the system's Hamiltonian were reviewed in detail.

Dissipative, in contrast to Hamiltonian, approaches to quantum state control in cavity optomechanics were investigated in chapter 2. The steady-state of those systems with different effective optomechanical couplings and under different driving conditions were investigated.

In chapter 3, a formalism for the description of multimode Gaussian states was described. A graphical and a compact algebraic description of these states was discussed.

In chapter 4, we described how tripartite entangled states could be prepared in a multimode cavity optomechanics setting. The effective Hamiltonian for our system was derived in the resolved-sideband regime. The required effective coupling rates between the electromagnetic cavity modes and the mechanical modes was derived, and hence the driving conditions for a specified target state were determined. Next the cavity mode was adiabatically eliminated from the system to create a description of the dynamics of the three mechanical oscillator alone. The dissipative operators of the three mechanical oscillators can be set to be the nullifiers of a continuous-variable tripartite cluster state. We explicitly considered two structures (linear and triangular tripartite cluster states) to study our tripartite entangled states.

In chapter 5, our findings on tripartite entangled mechanical oscillator state in multimode optomechanics were summarised. The steady-state was determined using a linear quantum systems theory approach. The presence of bipartite entanglement and genuine tripartite mechanical entanglement was determined. The impact of the mechanical motion on the spectrum of fluctuations of the coupled electromagnetic cavity modes was determined.

In summary, by carefully selecting the driving frequency, amplitude and phase of a multimode optomechanical system, we can prepare highly-entangled states of the multiple mechanical oscillators. The generation of such states has potential applications on sensing and quantum information processing.

6.2 Future Research

There are some prospective areas of research in related to our model of reservoir-engineered multimode cavity optomechanics. The potential future work includes:

- Limits of quantum mechanics $\longrightarrow$ This study arises the the fundamental question of quantum physics that, "Is there a limit to the size of systems to which one can apply quantum mechanics?" The dissipative control approaches described provide one route to answering this question experimentally.

- Quantum Many-Body Systems $\longrightarrow$ The research could be extended for arrays of mechanical oscillators coupled with one or multiple cavities in nonlinear many-body systems and optomechanical lattices. The long range entanglement properties of lattices of optomechanical systems need to be better understood.

Bibliography

[1] A. N. Cleland, *Foundations of Nanomechanics: From Solid-State Theory to Device Applications*. Springer Science & Business Media, 2013.

[2] J. Reddy, *Theory and Analysis of Elastic Plates*. Taylor and Francis, Philadelphia (PA), 1999.

[3] D. Karabacak, V. Yakhot, and K. Ekinci, "High-frequency nanofluidics: An experimental study using nanomechanical resonators," *Physical Review Letters*, vol. 98, no. 25, p. 254505, 2007.

[4] S. S. Verbridge, H. G. Craighead, and J. M. Parpia, "A megahertz nanomechanical resonator with room temperature quality factor over a million," *Applied Physics Letters*, vol. 92, no. 1, p. 13112, 2008.

[5] J. F. Vignola, J. A. Judge, J. Jarzynski, M. Zalalutdinov, B. H. Houston, and J. W. Baldwin, "Effect of viscous loss on mechanical resonators designed for mass detection," *Applied Physics Letters*, vol. 88, no. 4, p. 041921, 2006.

[6] G. Anetsberger, R. Rivière, A. Schliesser, O. Arcizet, and T. J. Kippenberg, "Ultralow-dissipation optomechanical resonators on a chip," *Nature Photonics*, vol. 2, no. 10, pp. 627–633, 2008.

[7] D. S. Bindel and S. Govindjee, "Elastic pmls for resonator anchor loss simulation," *International Journal for Numerical Methods in Engineering*, vol. 64, no. 6, p. 789, 2005.

[8] G. D. Cole, I. Wilson-Rae, K. Werbach, M. R. Vanner, and M. Aspelmeyer, "Phonon-tunnelling dissipation in mechanical resonators," *Nature Communications*, vol. 2, p. 231, 2011.

[9] M. Cross and R. Lifshitz, "Elastic wave transmission at an abrupt junction in a thin plate with application to heat transport and vibrations in mesoscopic systems," *Physical Review B*, vol. 64, no. 8, p. 085324, 2001.

[10] M. Eichenfield, J. Chan, R. M. Camacho, K. J. Vahala, and O. Painter, "Optomechanical crystals," *Nature*, vol. 462, no. 7269, p. 78, 2009.

[11] A. Jöckel, M. T. Rakher, M. Korppi, S. Camerer, D. Hunger, M. Mader, and P. Treutlein, "Spectroscopy of mechanical dissipation in micro-mechanical membranes," *Applied Physics Letters*, vol. 99, no. 14, p. 143109, 2011.

[12] J. A. Judge, D. M. Photiadis, J. F. Vignola, B. H. Houston, and J. Jarzynski, "Attachment loss of micromechanical and nanomechanical resonators in the limits of thick and thin support structures," *Journal of Applied Physics*, vol. 101, no. 1, p. 013521, 2007.

[13] T. Mattila, J. Kiihamäki, T. Lamminmäki, O. Jaakkola, P. Rantakari, A. Oja, H. Seppä, H. Kattelus, and I. Tittonen, "A 12 mhz micromechanical bulk acoustic mode oscillator," *Sensors and Actuators A: Physical*, vol. 101, no. 1, p. 1, 2002.

[14] Y.-H. Park and Y.-H. Park, "High-fidelity modeling of mems resonators. part i. anchor loss mechanisms through substrate," *Journal of Microelectromechanical Systems*, vol. 13, no. 2, p. 238, 2004.

[15] D. M. Photiadis and J. A. Judge, "Attachment losses of high q oscillators," *Applied Physics Letters*, vol. 85, no. 3, p. 482, 2004.

[16] K. Wang, A.-C. Wong, and C. T. Nguyen, "Vhf free-free beam high-q micromechanical resonators," *Journal of Microelectromechanical Systems*, vol. 9, no. 3, p. 347, 2000.

[17] I. Wilson-Rae, "Intrinsic dissipation in nanomechanical resonators due to phonon tunneling," *Physical Review B*, vol. 77, no. 24, p. 245418, 2008.

[18] A. Duwel, R. N. Candler, T. W. Kenny, and M. Varghese, "Engineering mems resonators with low thermoelastic damping," *Journal of Microelectromechanical Systems*, vol. 15, no. 6, p. 1437, 2006.

[19] A. Kiselev and G. Iafrate, "Phonon dynamics and phonon assisted losses in euler-bernoulli nanobeams," *Physical Review B*, vol. 77, no. 20, p. 205436, 2008.

[20] R. Lifshitz and M. L. Roukes, "Thermoelastic damping in micro-and nanomechanical systems," *Physical review B*, vol. 61, no. 8, p. 5600, 2000.

[21] P. Mohanty, D. Harrington, K. Ekinci, Y. Yang, M. Murphy, and M. Roukes, "Intrinsic dissipation in high-frequency micromechanical resonators," *Physical Review B*, vol. 66, no. 8, p. 085416, 2002.

[22] D. Southworth, R. Barton, S. Verbridge, B. Ilic, A. Fefferman, H. Craighead, and J. Parpia, "Stress and silicon nitride: A crack in the universal dissipation of glasses," *Physical Review Letters*, vol. 102, no. 22, p. 225503, 2009.

[23] Q. P. Unterreithmeier, T. Faust, and J. P. Kotthaus, "Damping of nanomechanical resonators," *Physical Review Letters*, vol. 105, no. 2, p. 027205, 2010.

[24] A. Venkatesan, K. Lulla, M. Patton, A. Armour, C. Mellor, and J. Owers-Bradley, "Dissipation due to tunneling two-level systems in gold nanomechanical resonators," *Physical Review B*, vol. 81, no. 7, p. 073410, 2010.

[25] K. Y. Yasumura, T. D. Stowe, E. M. Chow, T. Pfafman, T. W. Kenny, B. C. Stipe, and D. Rugar, "Quality factors in micron-and submicron-thick cantilevers," *Journal of Microelectromechanical Systems*, vol. 9, no. 1, p. 117, 2000.

[26] Y. Hadjar, P.-F. Cohadon, C. Aminoff, M. Pinard, and A. Heidmann, "High-sensitivity optical measurement of mechanical brownian motion," *Europhysics Letters*, vol. 47, no. 5, p. 545, 1999.

[27] H. Pleiner and H. R. Brand, "Hydrodynamics and electrohydrodynamics of liquid crystals," in *Pattern Formation in Liquid Crystals*, p. 15, Springer, 1996.

[28] A. Clerk, M. Devoret, S. Girvin, F. Marquardt, and R. Schoelkopf, "Introduction to quantum noise, measurement, and amplification," *Reviews of Modern Physics*, vol. 82, no. 2, p. 1155, 2010.

[29] C. Gardiner and P. Zoller, "Quantum noise," *Springer Series in Synergetics*, vol. 56.

[30] M. Woolley, A. Doherty, G. Milburn, and K. Schwab, "Nanomechanical squeezing with detection via a microwave cavity," *Physical Review A*, vol. 78, no. 6, p. 062303, 2008.

[31] E. Wollman, C. Lei, W. AJ, J. Suh, A. Kronwald, F. Marquardt, A. Clerk, and K. Schwab, "Quantum squeezing of motion in a mechanical resonator," *Science*, vol. 349, no. 6251, p. 952, 2015.

[32] A. Kronwald, F. Marquardt, and A. A. Clerk, "Arbitrarily large steady-state bosonic squeezing via dissipation," *Physical Review A*, vol. 88, p. 063833, 2013.

[33] A. Clerk, F. Marquardt, and K. Jacobs, "Back-action evasion and squeezing of a mechanical resonator using a cavity detector," *New Journal of Physics*, vol. 10, no. 9, p. 095010, 2008.

[34] M. Schlosshauer, *Decoherence: And the Quantum-to-Classical Transition*. Springer, Berlin, 2008.

[35] G. Lindblad, "On the generators of quantum dynamical semigroups," *Communications in Mathematical Physics*, vol. 48, no. 2, p. 119, 1976.

[36] M. G. A. Paris, F. Illuminati, A. Serafini, and S. De Siena, "Purity of gaussian states: Measurement schemes and time evolution in noisy channels," *Physical Review A*, vol. 68, no. 1, p. 012314, 2003.

[37] J. Teufel, T. Donner, D. Li, J. Harlow, M. Allman, K. Cicak, A. Sirois, J. D. Whittaker, K. Lehnert, and R. W. Simmonds, "Sideband cooling of micromechanical motion to the quantum ground state," *Nature*, vol. 475, no. 7356, p. 359, 2011.

[38] R. Kumar, E. Barrios, C. Kupchak, and A. I. Lvovsky, "Experimental characterization of bosonic creation and annihilation operators," *Physical Review Letter*, vol. 110, p. 130403, 2013.

[39] C. Gerry and P. Knight, *Introductory Quantum Optics*. Cambridge university press, 2005.

[40] L.-M. Duan, G. Giedke, J. I. Cirac, and P. Zoller, "Inseparability criterion for continuous variable systems," *Physical Review Letters*, vol. 84, p. 2722, 2000.

[41] A. Einstein, B. Podolsky, and N. Rosen, "Can quantum-mechanical description of physical reality be considered complete?," *Physical Review*, vol. 47, no. 10, p. 777, 1935.

[42] J. S. Bell, "On the einstein podolsky rosen paradox," 1964.

[43] M. F. Jensen, *A Comparison of French and Spanish Surrealist Poetics: A Cognitive Semiotic Approach into Breton, Éluard, Aleixandre, and Lorca*. PhD thesis, Case Western Reserve University, 2011.

[44] S. L. Braunstein, G. M. D'Ariano, G. J. Milburn, and M. F. Sacchi, "Universal teleportation with a twist," *Physical Review Letters*, vol. 84, no. 15, p. 3486, 2000.

[45] A. K. Ekert, "Quantum cryptography based on bells theorem," *Physical Review Letters*, vol. 67, no. 6, p. 661, 1991.

[46] R. Orús and J. I. Latorre, "Universality of entanglement and quantum-computation complexity," *Physical Review A*, vol. 69, no. 5, p. 052308, 2004.

[47] T. Opatrnỳ, B. Deb, and G. Kurizki, "Proposal for translational entanglement of dipole-dipole interacting atoms in optical lattices," *Physical Review Letters*, vol. 90, no. 25, p. 250404, 2003.

[48] C. Mejía-Monasterio, G. Benenti, G. G. Carlo, and G. Casati, "Entanglement across a transition to quantum chaos," *Physical Review A*, vol. 71, no. 6, p. 062324, 2005.

[49] L. Santos, G. Rigolin, and C. Escobar, "Entanglement versus chaos in disordered spin chains," *Physical Review A*, vol. 69, no. 4, p. 042304, 2004.

[50] S. Montangero, G. Benenti, and R. Fazio, "Dynamics of entanglement in quantum computers with imperfections," *Physical Review Letters*, vol. 91, no. 18, p. 187901, 2003.

[51] M. Arnesen, S. Bose, and V. Vedral, "Natural thermal and magnetic entanglement in the 1d heisenberg model," *Physical Review Letters*, vol. 87, no. 1, p. 017901, 2001.

[52] T. J. Osborne and M. A. Nielsen, "Entanglement in a simple quantum phase transition," *Physical Review A*, vol. 66, no. 3, p. 032110, 2002.

[53] G. Vidal, J. I. Latorre, E. Rico, and A. Kitaev, "Entanglement in quantum critical phenomena," *Physical review letters*, vol. 90, no. 22, p. 227902, 2003.

[54] T. S. Cubitt, F. Verstraete, and J. I. Cirac, "Entanglement flow in multipartite systems," *Physical Review A*, vol. 71, no. 5, p. 052308, 2005.

[55] G. Vidal, "Entanglement monotones," *Journal of Modern Optics*, vol. 47, no. 2-3, p. 355, 2000.

[56] C. H. Bennett, D. P. DiVincenzo, J. A. Smolin, and W. K. Wootters, "Mixed-state entanglement and quantum error correction," *Physical Review A*, vol. 54, no. 5, p. 3824, 1996.

[57] K. Życzkowski, P. Horodecki, A. Sanpera, and M. Lewenstein, "Volume of the set of separable states," *Physical Review A*, vol. 58, no. 2, p. 883, 1998.

[58] G. Vidal and R. F. Werner, "Computable measure of entanglement," *Physical Review A*, vol. 65, no. 3, p. 032314, 2002.

[59] M. B. Plenio, "Logarithmic negativity: a full entanglement monotone that is not convex," *Physical Review Letters*, vol. 95, no. 9, p. 090503, 2005.

[60] N. C. Menicucci, S. T. Flammia, and P. van Loock, "Graphical calculus for gaussian pure states," *Physical Review A*, vol. 83, no. 4, p. 042335, 2011.

[61] M. Gu, C. Weedbrook, N. C. Menicucci, T. C. Ralph, and P. van Loock, "Quantum computing with continuous-variable clusters," *Physical Review A*, vol. 79, no. 6, p. 062318, 2009.

[62] N. C. Menicucci, S. T. Flammia, H. Zaidi, and O. Pfister, "Ultracompact generation of continuous-variable cluster states," *Physical Review A*, vol. 76, no. 1, p. 010302, 2007.

[63] S. L. Braunstein and P. Van Loock, "Quantum information with continuous variables," *Reviews of Modern Physics*, vol. 77, no. 2, p. 513, 2005.

[64] A. Furusawa, J. L. Sørensen, S. L. Braunstein, C. A. Fuchs, H. J. Kimble, and E. S. Polzik, "Unconditional quantum teleportation," *Science*, vol. 282, no. 5389, p. 706, 1998.

[65] P. van Loock and S. L. Braunstein, "Unconditional teleportation of continuous-variable entanglement," *Physical Review A*, vol. 61, no. 1, p. 010302, 1999.

[66] M. Reid and P. Drummond, "Quantum correlations of phase in nondegenerate parametric oscillation," *Physical Review Letters*, vol. 60, no. 26, p. 2731, 1988.

[67] M. Reid, "Demonstration of the einstein-podolsky-rosen paradox using nondegenerate parametric amplification," *Physical Review A*, vol. 40, no. 2, p. 913, 1989.

[68] P. Drummond and M. Reid, "Correlations in nondegenerate parametric oscillation. ii. below threshold results," *Physical Review A*, vol. 41, no. 7, p. 3930, 1990.

[69] Z. Ou, S. F. Pereira, H. Kimble, and K. Peng, "Realization of the einstein-podolsky-rosen paradox for continuous variables," *Physical Review Letters*, vol. 68, no. 25, p. 3663, 1992.

[70] J. Zhang *et al.*, "Graphical description of local gaussian operations for continuous-variable weighted graph states," *Physical Review A*, vol. 78, no. 5, p. 052307, 2008.

[71] R. Simon, E. Sudarshan, and N. Mukunda, "Gaussian pure states in quantum mechanics and the symplectic group," *Physical Review A*, vol. 37, no. 8, p. 3028, 1988.

[72] N. C. Menicucci, P. van Loock, M. Gu, C. Weedbrook, T. C. Ralph, and M. A. Nielsen, "Universal quantum computation with continuous-variable cluster states," *Physical Review Letters*, vol. 97, no. 11, p. 110501, 2006.

[73] N. C. Menicucci, P. van Loock, M. Gu, C. Weedbrook, T. C. Ralph, and M. A. Nielsen, "Universal quantum computation with continuous-variable cluster states," *Physical Revew Letter*, vol. 97, p. 110501, 2006.

[74] S. D. Bartlett, B. C. Sanders, S. L. Braunstein, and K. Nemoto, "Efficient classical simulation of continuous variable quantum information processes," *Physical Review Letter*, vol. 88, p. 097904, 2002.

[75] J. Chan, T. M. Alegre, A. H. Safavi-Naeini, J. T. Hill, A. Krause, S. Gröblacher, M. Aspelmeyer, and O. Painter, "Laser cooling of a nanomechanical oscillator into its quantum ground state," *Nature*, vol. 478, no. 7367, p. 89, 2011.

[76] D. Vitali, P. Tombesi, M. Woolley, A. Doherty, and G. Milburn, "Entangling a nanomechanical resonator and a superconducting microwave cavity," *Physical Review A*, vol. 76, no. 4, p. 042336, 2007.

[77] D. Walls and G. J. Milburn, "Introduction," in *Quantum Optics*, p. 1, Springer, 2008.

[78] H. M. Wiseman and G. J. Milburn, "Quantum theory of field-quadrature measurements," *Physical review A*, vol. 47, no. 1, p. 642, 1993.

[79] L. Frunzio, A. Wallraff, D. Schuster, J. Majer, and R. Schoelkopf, "Fabrication and characterization of superconducting circuit qed devices for quantum computation," *IEEE Transactions on Applied Superconductivity*, vol. 15, no. 2, p. 860, 2005.

[80] M. LaHaye, O. Buu, B. Camarota, and K. Schwab, "Approaching the quantum limit of a nanomechanical resonator," *Science*, vol. 304, no. 5667, p. 74, 2004.

[81] J. Poyatos, J. Cirac, and P. Zoller, "Quantum reservoir engineering with laser cooled trapped ions," *Physical Review Letters*, vol. 77, no. 23, p. 4728, 1996.

[82] G.-x. Li, S.-s. Ke, and Z. Ficek, "Generation of pure continuous-variable entangled cluster states of four separate atomic ensembles in a ring cavity," *Physical Review A*, vol. 79, no. 3, p. 033827, 2009.

[83] K. Koga and N. Yamamoto, "Dissipation-induced pure gaussian state," *Physical Review A*, vol. 85, no. 2, p. 022103, 2012.

[84] G. Giedke, B. Kraus, M. Lewenstein, and J. I. Cirac, "Separability properties of three-mode gaussian states," *Physical Review A*, vol. 64, no. 5, p. 052303, 2001.

[85] G. Adesso, A. Serafini, and F. Illuminati, "Extremal entanglement and mixedness in continuous variable systems," *Physical Review A*, vol. 70, no. 2, p. 022318, 2004.

[86] G. Adesso, A. Serafini, and F. Illuminati, "Multipartite entanglement in three-mode gaussian states of continuous-variable systems: Quantification, sharing structure, and decoherence," *Physical Review A*, vol. 73, no. 3, p. 032345, 2006.